Energy-Efficient Deployment in Static and Mobile Heterogeneous Multi-Hop Wireless Sensor Networks

Saeed Karimi-Bidhendi, Jun Guo, and Hamid Jafarkhani

***Abstract*—We study a heterogeneous wireless sensor network (WSN) where N heterogeneous access points (APs) gather data from densely deployed sensors and transmit their sensed information to M heterogeneous fusion centers (FCs) via multi-hop wireless communication. The heterogeneous optimal deployment of APs and FCs is modeled as an optimization problem with total wireless communication power consumption of the network as its objective function. We consider both static WSNs, where APs and FCs retain their deployed position, and mobile WSNs where APs and FCs can move from their initial deployment to their optimal locations. Based on the derived necessary conditions for the optimal deployment in static WSNs, we propose an iterative algorithm to deploy APs and FCs. In addition, we study the necessary conditions of the optimal movement-efficient deployment in mobile WSNs with constrained movement energy and present iterative algorithms to find such deployments, accordingly. Simulation results show that our proposed deployment algorithms outperform the existing methods in the literature, and achieve a lower total wireless communication power in both static and mobile WSNs.**

***Index Terms*—Deployment, heterogeneous multi-hop networks, wireless sensor networks, power optimization.**

I. Introduction

Wireless sensor networks (WSNs) consist of small and low-cost sensor devices used to monitor the environment and transfer the sensed information through wireless channels to dedicated fusion centers. WSNs can be classified into either homogeneous WSNs [1]–[4], in which network nodes share the same characteristics such as storage, antennas, sensitivity etc., or heterogeneous WSNs where network nodes have different characteristics [5]–[10]. Based on the network architecture, WSNs can be divided into either hierarchical WSNs, where network nodes are often grouped into clusters with some of them chosen to be cluster heads, or non-hierarchical WSNs where sensors have identical functionality and multi-hop wireless communication is used to maintain the connectivity of the network. Wireless sensor nodes can also be classified as either static [7], [10], in which each network node remains at its deployed position, or mobile where network nodes can move to their optimal locations to improve the energy efficiency and sensing quality of WSNs [11]–[14]. In general, there are three fundamental elements to specify for a WSN: (i) node deployment, i.e., the location of network nodes; (ii) cell partitioning, i.e., the region that each network node monitors; and (iii) data routing, i.e., the path that each sensory data takes to reach fusion centers. Not only should a proper network design algorithm jointly optimize over node deployment, cell partitioning, and data routing, but also it should be applicable to heterogeneous WSNs and be extendable to both static and mobile network nodes.

In [1], [2], we studied the optimal deployment in homogeneous WSNs; however, the homogeneous setting does not address many challenges that are inherent in heterogeneous WSNs, e.g., unlike regular Voronoi diagrams in homogeneous WSNs, the optimal cells in heterogeneous WSNs may be non-convex, not star-shaped, or even disconnected and the cell boundaries may not be hyperplanes. In [5], [7], [9]–[11], we studied the energy-efficient deployment for heterogeneous WSNs; however, the network is restricted to a one-tiered or two-tiered architecture while an efficient data routing through multi-hop communication can substantially improve the total energy consumption. Thus, our prior studies along with the majority of the work in the literature, as we will explore in the next section, fall short on one or more of the desired properties discussed above; namely, they may not consider the heterogeneous nature of network nodes, lack a rigorous radio energy model for the communication energy consumption, assume a specific network architecture, and consider only a static or mobile setting.

The primary motivation and key characteristic of this work over the existing literature is that not only do we incorporate the heterogeneity of network nodes into our system model and make no assumption about the network's architecture, but also we consider a radio energy model, where the electromagnetic wave propagation dampens as a power law function of the distance between the transmitter and receiver, and develop deployment algorithms that are applicable to both static and mobile WSNs. In particular, we study the optimal deployment in heterogeneous multi-hop WSNs consisting of homogeneous densely deployed sensors, heterogeneous APs, and heterogeneous FCs, to minimize the wireless communication power consumption with and without movement energy constraints. Our contributions in this paper are multifold:

- We consider a radio energy model based on large scale fading and line-of-sight path loss signal attenuation that incorporates the heterogeneous characteristics of network nodes without any a priori assumption about the network's architecture, location of nodes, etc;
- We provide theoretical necessary conditions for an op-

Authors are with the Center for Pervasive Communications & Computing, University of California, Irvine, Irvine CA, 92697 USA (e-mail: {skarimib, guoj4, hamidj}@uci.edu). This work was presented in part at the 2020 IEEE International Conference on Communications [1]. This work was supported in part by the NSF Award CCF-1815339.

timal deployment, cell partitioning, and data routing design for both static and mobile heterogeneous WSNs to minimize the power consumption;
- We design energy-efficient algorithms to jointly optimize node deployment, cell partitioning, and data routing that satisfy the necessary conditions and prove their convergence.

The rest of the paper is organized as follows: In Section II, we present an overview of the existing literature on WSN deployment. In Section III, we provide the system model. In Section IV, we study the optimal deployment in static heterogeneous multi-hop WSNs and propose an iterative algorithm based on the derived necessary conditions. The analysis of optimal deployment with network's total movement energy constraint is provided in Section V. In Section VI, we study an energy-efficient deployment that guarantees a given network's lifetime in mobile WSNs. Experimental results are provided in Section VII and Section VIII concludes the paper.

II. Related Work

Energy efficiency is a key determinant in longevity of the WSNs since sensors have limited energy resources and it is difficult or infeasible to recharge the batteries of densely deployed sensors. In general, many factors contribute to the energy consumption of the WSNs, e.g., communication energy, movement energy, sensing energy, and computation energy [15], [16]. Empirical measurements have shown that the data processing and computation energy as well as sensing energy for passive sensors are negligible compared to communication energy [17]. Thus, wireless communication dominates the energy consumption in static sensors in practice while movement energy dominates the energy consumption in mobile wireless sensor networks [7], [18].

Several methods have been proposed in the literature to reduce the energy consumption of wireless communication in WSNs. Examples include methods that circumvent the excess energy consumption by appropriately switching sensors between awake and asleep states [19], calibrating the transmission power of sensors while a reliable communication is maintained [20], and finding optimal paths to transfer data from sensors to fusion centers [4]. The common drawback of these approaches is that the deployment is assumed to be known and fixed; however, because the required transmission power is polynomially proportional to the distance between the transmitter and the receiver, a proper deployment can significantly affect the energy consumption of WSNs.

There are two types of deployment techniques proposed in the literature to optimize the energy consumption of WSNs: random deployment and deterministic deployment. Random deployment is often used in harsh or inaccessible environments where deterministic deployment is not feasible. Examples include Constant Diffusion [21], Hybrid Diffusion [22], and Discontinuous Diffusion [23] in which network nodes are scattered in the target region according to a given probability density function. Since network nodes are not usually placed at their optimal locations due to the stochastic nature of these methods, the performance of random-based deployment falls short compared to the deterministic deployment. Deterministic deployment approaches aim to calculate the optimal location of network nodes that achieves a desired objective. These methods can be classified into four different categories, as we have summarized below:

1) *Grid-based methods:* Examples include [24], [25] in which the locations of network nodes are determined based on a grid shape such as triangular, rectangular, or hexagonal grid pattern. These methods are favorable due to their simplicity; however, they consider a homogeneous setting and do not account for the heterogeneity of network nodes; thus, they perform poorly when the WSN is comprised of nodes with different characteristics. In addition, they do not account for connectivity and are only applicable to static nodes.
2) *Force-based methods:* Examples include [26], [27] in which a set of attractive, repulsive or null virtual forces act on network nodes based on their distance from each other. These methods offer adequate coverage and are applicable to mobile nodes; however, they suffer from high computational complexity and do not scale well with the number of nodes. Moreover, they yield undesirable performance for heterogeneous WSNs since virtual forces do not consider the heterogeneity of nodes.
3) *Geometry-based methods:* Examples include Voronoi-based algorithms such as [28]–[30] in which the target region is partitioned into a set of unique polygons, one for each network node, such that each point within a polygon is closest to that network node compared to any other node residing in other polygons. While the intuition of closeness in the sense of Euclidean distance makes sense for homogeneous nodes, it has been shown to fail for heterogeneous WSNs in which the best partitioning heavily depends on nodes' characteristics [7]. Our proposed algorithms in this paper fall into this category of deployment methods.
4) *Meta-heuristic methods:* Examples include particle swarm optimization [31], genetic algorithm [32], and simulated annealing [33] in which various optimization tools are used to find nodes' locations. These methods are designed to achieve high coverage rates, but they are sensitive to node failure and suffer from high power consumption, high computational complexity, and low convergence rate. Additionally, fine-tuning the hyperparameters for these algorithms is very challenging since a slight variation can result in different network behavior.

To the best of our knowledge, the energy-efficient deployment in heterogeneous multi-hop WSNs is still an open problem. In the remainder of this paper, we study such networks in details.

III. System Model

In this section, we study the system model of heterogeneous multi-hop WSNs, as shown in Fig. 1, consisting of three types of network nodes: homogeneous sensors, heterogeneous APs, and heterogeneous FCs. Given the target region $\Omega \subseteq \mathbb{R}^2$ which is a convex polygon including its interior, N APs and M FCs are deployed to collect information from densely deployed

sensors. Let $\mathcal{I}_{\mathcal{A}} = \{1, \cdots, N\}$ and $\mathcal{I}_{\mathcal{F}} = \{N+1, \cdots, N+M\}$ denote the set of node indices for APs and FCs, respectively. Here, we refer to each access point or fusion center node as a point in the network, i.e., if $n \in \mathcal{I}_{\mathcal{A}}$, point n refers to AP n; however, when $n \in \mathcal{I}_{\mathcal{F}}$, point n refers to FC $(n-N)$. The location of point n is denoted by $p_n \in \Omega$ and collectively the deployment of APs and FCs is denoted by $\mathbf{P} = (p_1, \cdots, p_N, p_{N+1}, \cdots, p_{N+M}) \in \mathbb{R}^{(N+M)\times 2}$. Throughout this paper, we assume that each sensor only sends data to one AP; therefore, for each $n \in \mathcal{I}_{\mathcal{A}}$, AP n gathers data from sensors within the region $W_n \subseteq \Omega$ and $\mathbf{W} = (W_1, \cdots, W_N) \subseteq \Omega^N$ provides a set partitioning of the target region, i.e., we have $\bigcup_{n\in\mathcal{I}_{\mathcal{A}}} W_n = \Omega$ and $W_i \cap W_j = \varnothing$ for all $i, j \in \mathcal{I}_{\mathcal{A}}$ where $i \neq j$. The density of sensors is denoted via a continuous and differentiable function $f : \Omega \longrightarrow \mathbb{R}^+$, i.e., the number of densely deployed sensors within region W_n is equal to $\int_{W_n} f(\omega)d\omega$. The total amount of data collected from sensors within the region W_n in one time unit is $R_b \int_{W_n} f(\omega)d\omega$, where the bit-rate R_b is a constant due to the homogeneity of sensors [2]. For each $n \in \mathcal{I}_{\mathcal{A}}$, the volume and centroid of the region W_n is defined as $v(W_n) \triangleq \int_{W_n} f(\omega)d\omega$ and $c(W_n) \triangleq \frac{\int_{W_n} \omega f(\omega)d\omega}{\int_{W_n} f(\omega)d\omega}$, respectively. The data gathered from each sensor is forwarded to other APs or FCs in the network until it eventually reaches to one or more FCs.

As shown in Fig. 1, the network can be regarded as a directed acyclic graph $\mathcal{G}(\mathcal{I}_A \bigcup \mathcal{I}_F, \mathcal{E})$ where APs and FCs are source and sink nodes, respectively, and $\mathcal{E}$ is the set of directed edges (i, j) such that $i \in \mathcal{I}_{\mathcal{A}}$ and $j \in \mathcal{I}_{\mathcal{A}} \bigcup \mathcal{I}_{\mathcal{F}}$ [34]. Note that any cycle in the network's graph can be removed by reducing the flow of data along the cycle without changing the in-flow and out-flow links to that cycle. Let $\mathbf{F} = [F_{i,j}]_{N\times(N+M)}$ be the flow matrix, where $F_{i,j}$ is the amount of data transmitted through the link (i, j) in one time unit. Since the in-flow to each AP, say i, should be equal to the out-flow, we have $\sum_{j=1}^{N} F_{j,i} + R_b \int_{W_i} f(\omega)d\omega = \sum_{j=1}^{N+M} F_{i,j}$. For $i \in \mathcal{I}_{\mathcal{A}}$, we define $F_i \triangleq \sum_{j=1}^{N+M} F_{i,j}$ to be the total flow originated from AP i. Note that instead of directly specifying $F_{i,j}$, i.e., the amount of data transmitted from AP i to point j in one time unit, we can state the ratio of the total flow originated from AP i that goes to point j. In particular, let $\mathbf{S} = [s_{i,j}]_{N\times(N+M)}$ be the normalized flow matrix, where $s_{i,j} \triangleq \frac{F_{i,j}}{\sum_{j=1}^{N+M} F_{i,j}}$ is the ratio of the in-flow data to AP i that is transmitted to point j. The normalized flow matrix $\mathbf{S}$ satisfies the following properties: (a) $s_{i,j} \in [0, 1]$;[1] (b) $\sum_{j=1}^{N+M} s_{i,j} = 1$ because the in-flow to AP i should be equal to the out-flow, $\forall i \in \mathcal{I}_{\mathcal{A}}$; (c) No cycle: if there exists a path in the network's graph such as $l_0 \to l_1 \to \cdots \to l_K$, i.e., $\prod_{k=1}^{K} s_{l_{k-1},l_k} > 0$, then we have $s_{l_K,l_0} = 0$. In particular, we have $s_{i.i} = 0$, $\forall i \in \mathcal{I}_{\mathcal{A}}$. Since the flow matrix $\mathbf{F}$ can be uniquely determined by the set partitioning $\mathbf{W}$ and the normalized flow matrix $\mathbf{S}$, in the remaining of this paper, we use the notation $\mathbf{F}(\mathbf{W}, \mathbf{S})$ instead of $\mathbf{F}$. The example below describes how to calculate $\mathbf{F}(\mathbf{W}, \mathbf{S})$ in terms of $\mathbf{W}$ and $\mathbf{S}$.

[1]For time-invariant routing algorithms, such as Bellman-Ford Algorithm [35], the flows construct a tree-structured graph in which each network node has only one successor. Under such circumstances, the normalized flow from point i to point j is either 0 or 1, i.e., $s_{i,j} \in \{0, 1\}$. However, the time-variant routing algorithms, such as Flow Augmentation Algorithm [34], generate different flows during different time periods. As a result, the overall normalized flow from point i to point j can be a real number between 0 and 1, i.e., $s_{i,j} \in [0, 1]$.

Example 1. We consider the exemplary WSN depicted in Fig. 1 that consists of $N = 3$ APs and $M = 1$ FC. Given the bit-rate $R_b = 10$bps, the cell partitioning $\mathbf{W}$ with cell volumes $v(W_1) = 2$, $v(W_2) = 4$, $v(W_3) = 3$ and the normalized flow matrix $\mathbf{S} = \begin{bmatrix} 0 & 0.4 & 0.6 & 0 \\ 0 & 0 & 0.25 & 0.75 \\ 0 & 0 & 0 & 1 \end{bmatrix}$, the amount of data generated from sensors within each cell can be calculated as:

$$\Gamma(W_1) = R_b v(W_1) = 20\text{bps}, \ \Gamma(W_2) = R_b v(W_2) = 40\text{bps}, \\ \Gamma(W_3) = R_b v(W_3) = 30\text{bps}. \quad (1)$$

By definition, we have $F_i(\mathbf{W}, \mathbf{S}) = \Gamma(W_i) + \sum_{j=1}^{N} F_{j,i}(\mathbf{W}, \mathbf{S})$ and $F_{i,j}(\mathbf{W}, \mathbf{S}) = F_i(\mathbf{W}, \mathbf{S}) \times s_{i,j}$. Thus, it can be shown that $\mathbf{F} = [F_{i,j}]_{\substack{1\le i\le 3 \\ 1\le j\le 4}} = \begin{bmatrix} 0 & 8 & 12 & 0 \\ 0 & 0 & 12 & 36 \\ 0 & 0 & 0 & 54 \end{bmatrix}$ since we have:

$$F_{1,2}(\mathbf{W}, \mathbf{S}) = F_1(\mathbf{W}, \mathbf{S}) \times s_{1,2} = \Gamma(W_1) \times s_{1,2} = 8\text{bps}, \quad (2)$$

$$F_{2,3}(\mathbf{W}, \mathbf{S}) = F_2(\mathbf{W}, \mathbf{S}) \times s_{2,3} \\ = [\Gamma(W_2) + F_{1,2}(\mathbf{W}, \mathbf{S})] \times s_{2,3} = 12\text{bps}, \quad (3)$$

$$F_{2,4}(\mathbf{W}, \mathbf{S}) = F_2(\mathbf{W}, \mathbf{S}) \times s_{2,4} \\ = [\Gamma(W_2) + F_{1,2}(\mathbf{W}, \mathbf{S})] \times s_{2,4} = 36\text{bps}, \quad (4)$$

and the remaining elements of the flow matrix $\mathbf{F}$ can be calculated similarly.

In what follows, we formulate the wireless communication power consumption of the network. Also, we focus on the power consumption of sensors and APs, since FCs are usually supplied with reliable energy sources and their power consumption is not the main concern. We break down the network's power consumption into three components and elucidate them in depth: (i) Sensors' transmission power; (ii) APs' transmission power; and (iii) APs' receiver power. First, we focus on the sensor's power consumption. According to [2], due to the path-loss, the instant transmission power is equal to the square of the distance between the transmitter and the receiver multiplied by a constant that depends on their characteristics, i.e., $\eta \times \|p_n - \omega\|^2$ for a sensor positioned at ω that transmits its data to AP n, $n \in \mathcal{I}_{\mathcal{A}}$. As shown in [16], the power weight η is given by $\eta = \frac{P_{th}(4\pi)^2}{R_b G_t G_r \lambda_c^2}$, where P_{th} is the minimum receiver power threshold for successful reception, R_b is the bit-rate, G_t and G_r are the antenna gains of the transmitter and the receiver, respectively, and λ_c is the carrier signal wavelength. In the homogeneous setting, all nodes have the same characteristics; thus, the parameter η is the same and will not affect the optimization. However, in a heterogeneous multi-hop WSN, APs can have different antenna gains and SNR thresholds; hence, the parameter η will be a function of the AP's index. Therefore, the sensors' transmission power consumption can be written as

$$\overline{\mathcal{P}}_{\mathcal{S}}^{T}(\mathbf{P}, \mathbf{W}) = \sum_{n=1}^{N} \int_{W_n} \eta_n \|p_n - \omega\|^2 R_b f(\omega)d\omega. \quad (5)$$

Similarly, the instant transmission power from point i to point

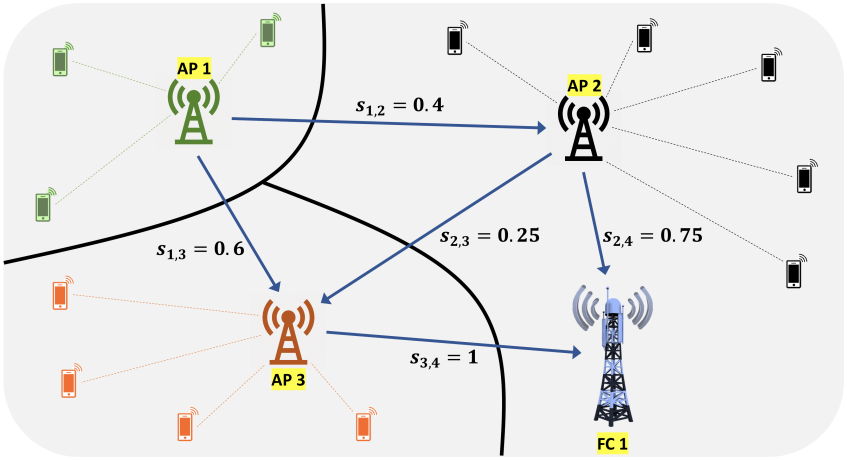

Fig. 1: An exemplary system model consisting of three APs and one FC. All network nodes corresponding to the same region are shown using the same color. Each sensor sends its collected data to its corresponding AP, as depicted via short dot lines. Each AP in turn transmits the gathered information to other APs or the FC, as shown via blue arrows, until all data eventually reach the deployed FC.

j can be written as $\beta \times \|p_i - p_j\|^2$ where the power weight β depends on the antenna gain and SNR threshold of point j and the antenna gain of point i [16]. Therefore, it is the same for the homogeneous setting and will not affect the optimization. However, in a heterogeneous multi-hop WSN, the heterogeneity of the APs and FCs causes the parameter β to be a function of their indices. Hence, the average transmission power through link (i, j) is equal to $\beta_{i,j}\|p_i - p_j\|^2 F_{i,j}(\mathbf{W}, \mathbf{S})$ and the APs' total transmission power consumption can be written as

$$\overline{\mathcal{P}}^T_{\mathcal{A}}(\mathbf{P}, \mathbf{W}, \mathbf{S}) = \sum_{i=1}^{N} \sum_{j=1}^{N+M} \beta_{i,j}\|p_i - p_j\|^2 F_{i,j}(\mathbf{W}, \mathbf{S}). \quad (6)$$

According to [6], power at the receiver of AP n can be modeled as $\sum_{i=1}^{N} \rho_n F_{i,n}(\mathbf{W}, \mathbf{S}) + \rho_n R_b \int_{W_n} f(\omega) d\omega$, where ρ_n is the power consumption coefficient for receiving data at AP n, and depends on digital coding, modulation, and filtering of the signal before transmission [16]. Therefore, the APs' total receiver power consumption can be written as:

$$\overline{\mathcal{P}}^R_{\mathcal{A}}(\mathbf{W}, \mathbf{S}) = \sum_{n=1}^{N} \rho_n \left[\sum_{i=1}^{N} F_{i,n}(\mathbf{W}, \mathbf{S}) + R_b \int_{W_n} f(\omega) d\omega \right]. \quad (7)$$

Thus, the total communication power consumption of the multi-hop WSN can be written as:

$$\mathcal{D}(\mathbf{P}, \mathbf{W}, \mathbf{S}) = \overline{\mathcal{P}}^T_{\mathcal{S}}(\mathbf{P}, \mathbf{W}) + \lambda \left[\overline{\mathcal{P}}^T_{\mathcal{A}}(\mathbf{P}, \mathbf{W}, \mathbf{S}) + \overline{\mathcal{P}}^R_{\mathcal{A}}(\mathbf{W}, \mathbf{S}) \right], \quad (8)$$

where the Lagrangian multiplier $\lambda \geq 0$ provides a trade-off between the sensor and AP power consumption. Our main objective in this paper is to minimize the multi-hop weighted communication power consumption defined in (8) over the deployment $\mathbf{P}$, cell partitioning $\mathbf{W}$, and the normalized flow matrix $\mathbf{S}$, which equivalently minimizes the weighted communication energy consumption of the network. Based on the system model and components of the objective function presented in this section, three specific problems are formulated in Sections IV, V, and VI below. Important notations used throughout this paper are summarized in Table I.

IV. Optimal Deployment in Static Heterogeneous Multi-Hop WSNs

As shown in (8), the total power consumption depends on three variables $\mathbf{P}$, $\mathbf{W}$, and $\mathbf{S}$ that conceptually represent locations, target region partitioning, and routing of data, respectively. Thus, our goal is to find the optimal AP and FC deployments, cell partitioning, and normalized flow matrix, denoted by $\mathbf{P}^* = (p_1^*, \cdots, p_N^*, p_{N+1}^*, \cdots, p_{N+M}^*)$, $\mathbf{W}^* = (W_1^*, \cdots, W_N^*)$, and $\mathbf{S}^* = [s_{i,j}^*]_{N \times (N+M)}$, respectively, that minimizes the multi-hop power consumption. Note that not only the variables $\mathbf{P}$, $\mathbf{W}$, and $\mathbf{S}$ are interdependent, i.e., the optimal value for each of them depends on the value of the other two variables, but also this optimization problem is NP-hard. Our aim is to derive the necessary conditions for optimal deployment and design an algorithm that iterates between three steps where in each step the value of one variable is optimized while the other two variables are held fixed.

Step 1 [optimizing $\mathbf{W}$ while $\mathbf{P}$ and $\mathbf{S}$ are fixed]: First we need to introduce a few concepts. In order to determine the energy required by each AP to transmit its data to FCs, without loss of generality, we assume that AP n's gathered data goes through K_n paths in the network's graph before it reaches to one or more fusion centers. We denote these paths by $\left\{L_k^{(n)}(\mathbf{S})\right\}_{k \in \{1, \cdots, K_n\}}$, where $L_k^{(n)}(\mathbf{S}) = l_{k,0}^{(n)} \rightarrow l_{k,1}^{(n)} \rightarrow \cdots \rightarrow l_{k,J_k^{(n)}}^{(n)}$, $l_{k,0}^{(n)} = n$, $l_{k,i}^{(n)} \in \mathcal{I}_{\mathcal{A}}$ for $i \in \{0, \cdots, J_k^{(n)} - 1\}$, $l_{k,J_k^{(n)}}^{(n)} \in \mathcal{I}_{\mathcal{F}}$ and $J_k^{(n)}$ is the number of hops on the k-th path. The portion of the total flow originated from AP n that goes through the k-th path can then be calculated as

$$\mu_k^{(n)}(\mathbf{W}, \mathbf{S}) = F_n(\mathbf{W}, \mathbf{S}) \prod_{i=1}^{J_k^{(n)}} s_{l_{k,i-1}^{(n)}, l_{k,i}^{(n)}}. \quad (9)$$

TABLE I: Important notations

Symbol	Description	Symbol	Description
$\mathbf{P}$	Location of APs and FCs	g_n	AP n's power coefficient
$\mathbf{W}$	Target region partitioning	ζ_n	Moving cost parameter
$\mathbf{S}$	Normalized flow matrix	λ	Lagrangian multiplier
$\mathbf{F}$	Flow matrix	γ	Maximum movement energy
$\mathcal{D}$	Communication power consumption	γ_n	Individual movement energy
$\overline{\mathcal{P}}_{\mathcal{S}}^{T}$	Sensor transmission power	η_n	Power weight for AP n
$\overline{\mathcal{P}}_{\mathcal{A}}^{T}$	AP transmission power	$\beta_{i,j}$	Power weight for points i,j
$\overline{\mathcal{P}}_{\mathcal{A}}^{R}$	AP receiver power	ρ_n	Receiver power coefficient

In particular, we have $\sum_{k=1}^{K_n}\mu_k^{(n)}(\mathbf{W},\mathbf{S}) = F_n(\mathbf{W},\mathbf{S})$ that indicates the data from AP n eventually reaches to one or more FCs. Next, for each link (i,j) in the network's graph, we define the energy cost (Joules/bit) to be:

$$e_{i,j}(\mathbf{P}) \triangleq \begin{cases}\beta_{i,j}\|p_i-p_j\|^2+\rho_j, & \text{if } j\in\mathcal{I}_{\mathcal{A}}\\ \beta_{i,j}\|p_i-p_j\|^2, & \text{if } j\in\mathcal{I}_{\mathcal{F}}.\end{cases} \tag{10}$$

Hence, we define the path cost corresponding to the k-th path from AP n to FCs as:

$$\overline{e}_k^{(n)}(\mathbf{P},\mathbf{S}) = \sum_{i=1}^{J_k^{(n)}} e_{l_{k,i-1}^{(n)},l_{k,i}^{(n)}}(\mathbf{P}). \tag{11}$$

Note that $\mu_k^{(n)}(\mathbf{W},\mathbf{S})$ is the portion of data collected by AP n that goes through the $k-$th path until reaching fusion centers and $\mu_k^{(n)}(\mathbf{W},\mathbf{S})\,\overline{e}_k^{(n)}(\mathbf{P},\mathbf{S})$ is the required power for this portion of data to travel through the $k-$th path. Now, AP n's power coefficient, denoted by $g_n(\mathbf{P},\mathbf{S})$ is defined to be the energy consumption (Joules/bit) for transmitting 1 bit data from AP n to the FCs, i.e., we have:

$$g_n(\mathbf{P},\mathbf{S}) = \frac{\sum_{k=1}^{K_n}\mu_k^{(n)}(\mathbf{W},\mathbf{S})\,\overline{e}_k^{(n)}(\mathbf{P},\mathbf{S})}{F_n(\mathbf{W},\mathbf{S})} \tag{12}$$

$$= \sum_{k=1}^{K_n}\left[\prod_{i=1}^{J_k^{(n)}} s_{l_{k,i-1}^{(n)},l_{k,i}^{(n)}}\left(\sum_{j=1}^{J_k^{(n)}}\beta_{l_{k,j-1}^{(n)},l_{k,j}^{(n)}}\left\|p_{l_{k,j-1}^{(n)}}-p_{l_{k,j}^{(n)}}\right\|^2 + \sum_{j=1}^{J_k^{(n)}-1}\rho_{l_{k,j}^{(n)}}\right)\right]. \tag{13}$$

Note that the term $F_n(\mathbf{W},\mathbf{S})$ is canceled in (12), implying that power coefficient $g_n(\mathbf{P},\mathbf{S})$ is independent of $\mathbf{W}$. The following example shows how to calculate the AP power coefficients.

Example 2. Consider the WSN described in Example 1 and let $\mathbf{P} = ((0,0),(0,1),(1,0),(1,1))$, $\beta_{i,j}=1$, and $\rho_i=1$ for all $i\in\mathcal{I}_{\mathcal{A}}$ and $j\in\mathcal{I}_{\mathcal{A}}\bigcup\mathcal{I}_{\mathcal{F}}$. We aim to find AP 1's power coefficient $g_1(\mathbf{P},\mathbf{S})$. The link energy costs for this network can be calculated as $e_{1,2}(\mathbf{P})=e_{1,3}(\mathbf{P})=2$, $e_{2,3}(\mathbf{P})=3$, and $e_{2,4}(\mathbf{P})=e_{3,4}(\mathbf{P})=1$. Note that AP 1's data goes through the following 3 paths: $L_1^{(1)}(\mathbf{S})=1\to2\to4$, $L_2^{(1)}(\mathbf{S})=1\to3\to4$, and $L_3^{(1)}(\mathbf{S})=1\to2\to3\to4$. The data rate through the above paths are, respectively, $\mu_1^{(1)}(\mathbf{W},\mathbf{S})=F_1(\mathbf{W},\mathbf{S})\times s_{1,2}\times s_{2,4}=0.3F_1(\mathbf{W},\mathbf{S})$, $\mu_2^{(1)}(\mathbf{W},\mathbf{S})=F_1(\mathbf{W},\mathbf{S})\times s_{1,3}\times s_{3,4}=0.6F_1(\mathbf{W},\mathbf{S})$, and $\mu_3^{(1)}(\mathbf{W},\mathbf{S})=F_1(\mathbf{W},\mathbf{S})\times s_{1,2}\times s_{2,3}\times s_{3,4}=0.1F_1(\mathbf{W},\mathbf{S})$. Moreover, we can calculate the path costs using (11) as follows: $\overline{e}_1^{(1)}(\mathbf{P})=e_{1,2}(\mathbf{P})+e_{2,4}(\mathbf{P})=3$, $\overline{e}_2^{(1)}(\mathbf{P})=e_{1,3}(\mathbf{P})+e_{3,4}(\mathbf{P})=3$, and $\overline{e}_3^{(1)}(\mathbf{P})=e_{1,2}(\mathbf{P})+e_{2,3}(\mathbf{P})+e_{3,4}(\mathbf{P})=6$. Then, AP 1's power coefficient is $g_1(\mathbf{P},\mathbf{S})=0.3\times3+0.6\times3+0.1\times6=3.3$.

To derive the necessary condition for an optimal cell partitioning, first, we need to rewrite the objective function in (8).

Lemma 1: For the AP power coefficient defined in (12), we have:

$$\sum_{n=1}^{N} g_n(\mathbf{P},\mathbf{S})\,R_b\int_{W_n} f(\omega)d\omega = \tag{14}$$

$$\sum_{i=1}^{N}\left[\sum_{j=1}^{N+M}\beta_{i,j}\|p_i-p_j\|^2F_{i,j}(\mathbf{W},\mathbf{S})+\sum_{j=1}^{N}\rho_jF_{i,j}(\mathbf{W},\mathbf{S})\right].$$

The proof is provided in Appendix A. Using Lemma 1, the objective function is:

$$\mathcal{D}(\mathbf{P},\mathbf{W},\mathbf{S}) = \sum_{n=1}^{N}\int_{W_n}\Big(\eta_n\|p_n-\omega\|^2R_b+\lambda g_n(\mathbf{P},\mathbf{S})\,R_b + \lambda\rho_nR_b\Big)f(\omega)d\omega. \tag{15}$$

Now, we study the properties of the optimal cell partitioning. For each $n\in\mathcal{I}_{\mathcal{A}}$, the Voronoi cell $\mathcal{V}_n$ for a deployment $\mathbf{P}$ and normalized flow matrix $\mathbf{S}$ is defined to be:

$$\mathcal{V}_n(\mathbf{P},\mathbf{S}) \triangleq \big\{\omega:\eta_n\|p_n-\omega\|^2+\lambda g_n(\mathbf{P},\mathbf{S})+\lambda\rho_n \le \eta_k\|p_k-\omega\|^2+\lambda g_k(\mathbf{P},\mathbf{S})+\lambda\rho_k,\forall k\neq n\big\}. \tag{16}$$

Ties are broken in the favor of the smaller index to ensure that each Voronoi cell $\mathcal{V}_n$ is a Borel set. For brevity, we write $\mathcal{V}_n$ instead of $\mathcal{V}_n(\mathbf{P},\mathbf{S})$ when it is clear from the context. The collection

$$\mathcal{V}(\mathbf{P},\mathbf{S}) = (\mathcal{V}_1,\mathcal{V}_2,\cdots,\mathcal{V}_N) \tag{17}$$

is referred to as the generalized Voronoi diagram [7]. Note that in contrast to the regular Voronoi diagrams, the Voronoi cells defined in (16) can be non-convex, not star-shaped, and even disconnected. The following proposition indicates that given a deployment $\mathbf{P}$ and normalized flow matrix $\mathbf{S}$, the generalized Voronoi diagram provides the optimal cell partitioning.

Proposition 1: For any deployment $\mathbf{P}$, cell partitioning $\mathbf{W}$,

and normalized flow matrix $\mathbf{S}$, we have:

$$\mathcal{D}\left(\mathbf{P},\mathbf{W},\mathbf{S}\right) \geq \mathcal{D}\left(\mathbf{P},\mathcal{V}\left(\mathbf{P},\mathbf{S}\right),\mathbf{S}\right). \tag{18}$$

The proof is provided in Appendix B.

Step 2 [optimizing S while P and W are fixed]: Now, given the link costs $\{e_{i,j}\left(\mathbf{P}\right)\}$s and generated sensing data rate from each cell partition, the total multi-hop power consumption can be minimized by Bellman-Ford Algorithm [35]. For convenience, we show the functionality of Bellman-Ford Algorithm by $\mathbf{S} = \mathcal{R}\left(\mathbf{P},\mathbf{W}\right)$, i.e., $\mathcal{R}\left(\mathbf{P},\mathbf{W}\right) = \arg\min_{\mathbf{S}} \left[\overline{\mathcal{P}}_{\mathcal{A}}^{T}\left(\mathbf{P},\mathbf{W},\mathbf{S}\right) + \overline{\mathcal{P}}_{\mathcal{A}}^{R}\left(\mathbf{W},\mathbf{S}\right)\right]$. Since the sensors' power consumption is independent of $\mathbf{S}$, we have:

$$\begin{aligned}\mathcal{R}(\mathbf{P},\mathbf{W}) &= \arg\min_{\mathbf{S}} \overline{\mathcal{P}}_{\mathcal{S}}^{T}(\mathbf{P},\mathbf{W}) \\ &\qquad + \lambda\left[\overline{\mathcal{P}}_{\mathcal{A}}^{T}(\mathbf{P},\mathbf{W},\mathbf{S}) + \overline{\mathcal{P}}_{\mathcal{A}}^{R}(\mathbf{W},\mathbf{S})\right] \\ &= \arg\min_{\mathbf{S}} \mathcal{D}(\mathbf{P},\mathbf{W},\mathbf{S}).\end{aligned} \tag{19}$$

Hence, the optimal flow matrix for a given $\mathbf{P}$ and $\mathbf{W}$ is $\mathbf{F}\left(\mathbf{W},\mathcal{R}\left(\mathbf{P},\mathbf{W}\right)\right)$.

Step 3 [optimizing P while W and S are fixed]: For notational brevity, we define the point $z_i\left(\mathbf{P},\mathbf{W},\mathbf{S}\right)$, or z_i for short, to be:

$$z_i = \frac{\eta_i R_b v_i c_i + \lambda\left(\sum_{j=1}^{N+M}\beta_{i,j}F_{i,j}p_j + \sum_{j=1}^{N}\beta_{j,i}F_{j,i}p_j\right)}{\eta_i R_b v_i + \lambda\left(\sum_{j=1}^{N+M}\beta_{i,j}F_{i,j} + \sum_{j=1}^{N}\beta_{j,i}F_{j,i}\right)}, \tag{20}$$

for all $i \in \mathcal{I}_{\mathcal{A}}$, and

$$z_i = \frac{\sum_{j=1}^{N}\beta_{j,i}F_{j,i}p_j}{\sum_{j=1}^{N}\beta_{j,i}F_{j,i}}, \tag{21}$$

for all $i \in \mathcal{I}_{\mathcal{F}}$. The following theorem provides the necessary conditions for the optimal deployment.

Proposition 2: The necessary conditions for the optimal deployments in heterogeneous multi-hop WSNs with communication power consumption defined in (8) are

$$p_i^* = z_i^*, \qquad \forall i \in \mathcal{I}_{\mathcal{A}} \bigcup \mathcal{I}_{\mathcal{F}} \tag{22}$$

$$\mathbf{W}^* = \mathcal{V}\left(\mathbf{P}^*,\mathbf{S}^*\right), \tag{23}$$

$$\mathbf{S}^* = \mathcal{R}\left(\mathbf{P}^*,\mathbf{W}^*\right), \tag{24}$$

where $z_i^* = z_i\left(\mathbf{P}^*,\mathbf{W}^*,\mathbf{S}^*\right)$ is given by Eqs. (20) and (21). The proof of Proposition 2 is provided in Appendix C. In what follows, first, we quickly review the conventional Lloyd Algorithm [36]. Lloyd Algorithm iterates between two steps: (i) Voronoi partitioning and (ii) Moving each node to the geometric centroid of its corresponding Voronoi region. Although the conventional Lloyd Algorithm can be used for one-tier quantizers or one-tier deployment tasks [10], it cannot be applied to WSNs with multi-hop wireless communications. Based on the properties explored in this section, we propose a Routing-aware Lloyd (RL) Algorithm, as outlined in Algorithm 1, to optimize the deployment in static heterogeneous multi-hop WSNs and minimize the objective function in (8). The proof of convergence for the RL algorithm is similar to that of other Lloyd-like algorithms [37].

Algorithm 1: Routing-aware Lloyd Algorithm

Result: Optimal deployment $\mathbf{P}$, cell partitioning $\mathbf{W}$, and normalized flow matrix $\mathbf{S}$.
Input: Convergence error threshold $\epsilon \in \mathbb{R}^{+}$;
do
– Calculate the objective function $\mathcal{D}_{\text{old}} = \mathcal{D}\left(\mathbf{P},\mathbf{W},\mathbf{S}\right)$;
1. Update the cell partitioning $\mathbf{W}$ according to Eq. (23);
2. Update the normalized flow matrix $\mathbf{S}$ using to the Bellman-Ford algorithm;
3. Update the deployment $\mathbf{P} = (p_1, \cdots, p_{N+M})$ according to Eq. (22);
– Calculate the objective function $\mathcal{D}_{\text{new}} = \mathcal{D}\left(\mathbf{P},\mathbf{W},\mathbf{S}\right)$;
while $\frac{\mathcal{D}_{\text{old}} - \mathcal{D}_{\text{new}}}{\mathcal{D}_{\text{old}}} \geq \epsilon$;

Finally, we analyze the time complexity of the RL algorithm. The Bellman-Ford algorithm runs in $\tau = \mathcal{O}\left(|\mathcal{I}_{\mathcal{A}} \cup \mathcal{I}_{\mathcal{F}}| \times |\mathcal{E}|\right)$ time for each AP $n \in \{1, \cdots, N\}$, which is also the time needed to calculate the power coefficient of AP n, i.e., g_n. Note that for a fixed number of iterations and sensor grid size, Eqs. (22), (23), and (24) are dominated by $\mathcal{O}\left(N\tau\right)$ time complexity; thus, RL Algorithm runs in $\mathcal{O}\left(N \times (N+M) \times \left[\binom{N}{2} + NM\right]\right) = \mathcal{O}\left(N^2(N+M)^2\right)$ time.

V. Optimal Deployment with a Total Energy Constraint in Mobile WSNs

A. Problem formulation

In Section IV, we considered the scenario in which APs and FCs can be directly placed at the optimal locations calculated via RL Algorithm. However, here we study mobile heterogeneous multi-hop WSNs in which each node moves from its initial position to its optimal location that minimizes the communication power consumption in (8) while the total movement energy consumption of the network is constrained. More precisely, given the linear model for movement energy consumption [38], for $n \in \mathcal{I}_{\mathcal{A}} \bigcup \mathcal{I}_{\mathcal{F}}$, point n's movement energy can be modeled as:

$$E_n\left(\mathbf{P}\right) = \zeta_n \|p_n - \tilde{p}_n\|, \tag{25}$$

where the moving cost parameter ζ_n depends on point n's energy efficiency, p_n and $\tilde{p}_n$ are its destination and initial locations, respectively. Therefore, the total movement energy consumption of the network is

$$E\left(\mathbf{P}\right) = \sum_{n=1}^{N+M} E_n\left(\mathbf{P}\right) = \sum_{n=1}^{N+M} \zeta_n \|p_n - \tilde{p}_n\|. \tag{26}$$

Our main objective in this section is to find the optimal node deployment, cell partitioning, and normalized flow matrix that minimizes the communication power consumption in Eq. (8) while the total movement energy is limited, i.e., the constrained optimization problem is defined as

$$\underset{\mathbf{P},\mathbf{W},\mathbf{S}}{\text{minimize}}\, \mathcal{D}\left(\mathbf{P},\mathbf{W},\mathbf{S}\right), \tag{27}$$

$$\text{s.t.} \qquad E\left(\mathbf{P}\right) \leq \gamma \tag{28}$$

where $\gamma \geq 0$ is the maximum movement energy consumption of the network.

B. Optimal Deployment

The movement energy in (28) is independent of the cell partitioning and normalized flow matrix; therefore, the generalized Voronoi diagram and Bellman-Ford Algorithm, represented in Eqs. (17) and (19), respectively, still provide the optimal cell partitioning and normalized flow matrix. Therefore, we only need to discuss the optimal deployment for the constrained optimization problem in Eqs. (27) and (28).

Lemma 2: Let $\mathbf{P}^*$, $\mathbf{W}^*$, and $\mathbf{S}^*$ be the optimal deployment, cell partitioning, and normalized flow matrix for the constrained optimization problem in Eqs. (27) and (28). We have:

$$p_i^* = \delta_i \tilde{p}_i + (1-\delta_i) \times z_i^*, \qquad \forall i \in \mathcal{I}_{\mathcal{A}} \bigcup \mathcal{I}_{\mathcal{F}} \tag{29}$$

where $\delta_i \in [0,1]$ and $\tilde{p}_i$ is the initial location of point i.
The proof is provided in Appendix D. Lemma 2 states that the optimal location for point i is on the line connecting its initial position to the point $z_i^* = z_i\left(\mathbf{P}^*,\mathbf{W}^*,\mathbf{S}^*\right)$. Note that this is in contrast to the optimal deployment without movement energy constraint in Section IV, i.e., $p_i^* = z_i^*$, as shown in Proposition 2. The difference is because of the constraint in Eq. (28). Intuitively, for $\gamma = 0$, we have $\delta_i = 1$ for all $i \in \mathcal{I}_{\mathcal{A}} \bigcup \mathcal{I}_{\mathcal{F}}$, i.e., each AP or FC will remain at its initial position since there is zero total available movement energy. However, for sufficiently large enough γ, we have $\delta_i = 0$, i.e., $p_i^* = z_i^*$ for all $i \in \mathcal{I}_{\mathcal{A}} \bigcup \mathcal{I}_{\mathcal{F}}$. In general, APs and FCs can be classified into two groups based on whether they have positive moving distance or they stand still. Let $\mathcal{I}_d = \{n \mid \|p_n - \tilde{p}_n\| > 0, \forall n \in \mathcal{I}_{\mathcal{A}} \bigcup \mathcal{I}_{\mathcal{F}}\}$ and $\mathcal{I}_s = \{n \mid \|p_n - \tilde{p}_n\| = 0, \forall n \in \mathcal{I}_{\mathcal{A}} \bigcup \mathcal{I}_{\mathcal{F}}\}$ be the set of dynamic and static points, respectively. Below we provide the necessary condition for the optimal deployment in multi-hop WSNs with total movement energy constraint:

Proposition 3: Let $\mathbf{P}^*, \mathbf{W}^*$, and $\mathbf{S}^*$ be the optimal deployment, cell partitioning, and normalized flow matrix for the constrained optimization problem in Eqs. (27) and (28). Then:

$$\chi_n^* = \chi_m^* \geq \chi_k^*, \qquad \forall n,m \in \mathcal{I}_d, k \in \mathcal{I}_s \tag{30}$$

$$p_n^* = \tilde{p}_n + \Gamma_n^* \times r_n^*, \qquad \forall n \in \mathcal{I}_d \tag{31}$$

where $r_n^* = 1 - \frac{\max\left(0, \sum_{i\in\mathcal{I}_d} \zeta_i \|\Gamma_i^*\| - \gamma\right)}{\|\Gamma_n^*\| \times \frac{\psi_n^*}{\zeta_n} \times \sum_{i\in\mathcal{I}_d} \frac{\zeta_i^2}{\psi_i^*}}$, $\Gamma_n^* = z_n^* - \tilde{p}_n$, and ψ_n^* is defined to be

$$\psi_n^* \triangleq \begin{cases} \eta_n R_b v_n^* + \lambda \left[\sum\limits_{k=1}^{N+M} \beta_{n,k} F_{n,k}^* + \sum\limits_{k=1}^{N} \beta_{k,n} F_{k,n}^* \right], & \forall n \in \mathcal{I}_{\mathcal{A}} \\ \lambda \sum\limits_{k=1}^{N} \beta_{k,n} F_{k,n}^*, & \forall n \in \mathcal{I}_{\mathcal{F}} \end{cases} \tag{32}$$

and the moving efficiency χ_n^* is defined as

$$\chi_n^* = \frac{\psi_n^* \|p_n^* - z_n^*\|^2}{\zeta_n \|p_n^* - z_n^*\|} = \frac{\psi_n^*}{\zeta_n} \|p_n^* - z_n^*\|, \ \forall n \in \mathcal{I}_{\mathcal{A}} \bigcup \mathcal{I}_{\mathcal{F}} \tag{33}$$

to reflect point n's ability to reduce the communication power consumption by movement.
The proof is provided in Appendix E. Proposition 3 captures the intuition in Lemma 2 that in an optimal deployment, point n is located on the line connecting its initial position $\tilde{p}_n$ to the point z_n^*, for all $n \in \mathcal{I}_{\mathcal{A}} \bigcup \mathcal{I}_{\mathcal{F}}$. Furthermore, for a sufficiently large enough available movement energy γ, say $\gamma \geq \sum_{i\in\mathcal{I}_d} \zeta_i \|\Gamma_i^*\|$, we have $p_n^* = z_n^*$ for all $n \in \mathcal{I}_d$ which reduces Proposition 3 to the necessary condition given by Eq. (22) for static WSNs. Based on the necessary conditions in Proposition 3, we propose a Movement-Efficient Routing-aware Lloyd (MERL) Algorithm, as outlined in Algorithm 2, to optimize the deployment in heterogeneous multi-hop WSNs with constrained movement energy and minimize the objective function in Eqs. (27) and (28). The proof of convergence for the MERL algorithm is similar to that of the RL algorithm [37].

Algorithm 2: Movement-Efficient Routing-aware Lloyd Algorithm

Result: Optimal deployment $\mathbf{P}$, cell partitioning $\mathbf{W}$, and normalized flow matrix $\mathbf{S}$.
Input: Initial deployment $\tilde{\mathbf{P}}$, convergence error threshold $\epsilon \in \mathbb{R}^+$;
do
– Calculate the objective function $\mathcal{D}_{\text{old}} = \mathcal{D}\left(\mathbf{P},\mathbf{W},\mathbf{S}\right)$;
1. Update the cell partitioning $\mathbf{W}$ according to Eq. (23);
2. Update the normalized flow matrix $\mathbf{S}$ using the Bellman-Ford algorithm;
3. Set $\mathcal{I}_d = \{1, \cdots, N+M\}$ and calculate r_n for all $n \in \mathcal{I}_d$;
4. while $\exists n \in \mathcal{I}_d$ such that $r_n \leq 0$ **do**
4.1. Update $\mathcal{I}_d = \mathcal{I}_d - \bigcup_{r_n \leq 0} n$;
4.2. Update $\{r_n\}_{n\in\mathcal{I}_d}$;
end
5. Update p_n for all $n \in \mathcal{I}_d$ using Eq. (31);
– Calculate the objective function $\mathcal{D}_{\text{new}} = \mathcal{D}\left(\mathbf{P},\mathbf{W},\mathbf{S}\right)$;
while $\frac{\mathcal{D}_{\text{old}} - \mathcal{D}_{\text{new}}}{\mathcal{D}_{\text{old}}} \geq \epsilon$;

VI. Optimal Deployment with a Network Lifetime Constraint in Mobile WSNs

A. Problem formulation

In Section V, we considered the deployment problem with a total movement energy constraint, which can be seen as a resource allocation problem. In this section, we focus on minimizing the communication power consumption given a constraint on the network lifetime. Let ν_n be the total energy of AP n or FC n and α_n be the communication power consumption of point n after relocation. To ensure a network

TABLE II: Simulation parameters

minimum received power (nW)				electronics energy dissipation (nJ/bit)		
$\mathbf{P_{th_{1:15}}}$	$\mathbf{P_{th_{16:30}}}$	$\mathbf{P_{th_{31}}}$	$\mathbf{P_{th_{32:33}}}$	$\rho_{\mathbf{1:7}}$	$\rho_{\mathbf{8:16}}$	$\rho_{\mathbf{17:30}}$
10	6	6	10	40	50	60

TABLE III: Transmitter and receiver antenna gains

transmitter antenna gain		receiver antenna gain	
$\mathbf{G_{t_{1:7,15:22}}}$	$\mathbf{G_{t_{8:14,23:30}}}$	$\mathbf{G_{r_{1:3,8:11,15:18,23:26,31:32}}}$	$\mathbf{G_{r_{4:7,12:14,19:22,27:30,33}}}$
1	2	1	2

lifetime of T after relocation, we should keep at least $\alpha_n T$ energy for communication. As a result, the following condition has to be satisfied:

$$\nu_n - E_n(\mathbf{P}) \geq \alpha_n T, \qquad \forall n \in \mathcal{I}_{\mathcal{A}} \bigcup \mathcal{I}_{\mathcal{F}}. \tag{34}$$

Hence, the network lifetime of T can be achieved by setting a maximum individual movement energy consumption for each AP or FC. Here, our main objective is to find the optimal deployment for the following constrained optimization problem:

$$\underset{\mathbf{P},\mathbf{W},\mathbf{S}}{\text{minimize}}\, \mathcal{D}(\mathbf{P},\mathbf{W},\mathbf{S}) \tag{35}$$

$$\text{s.t.} \qquad E_n(\mathbf{P}) \leq \gamma_n, \qquad \forall n \in \mathcal{I}_{\mathcal{A}} \bigcup \mathcal{I}_{\mathcal{F}} \tag{36}$$

where $\gamma_n = \nu_n - \alpha_n T$ is the maximum individual movement energy consumption of point n.

B. Optimal Deployment

Here, our goal is to find the optimal deployment $\mathbf{P}^*$, cell partitioning $\mathbf{W}^*$, and normalized flow matrix $\mathbf{S}^*$ that minimizes the multi-hop communication power consumption while each individual movement energy consumption is constrained. The following theorem provides the necessary condition for optimal deployment in the constrained optimization problem in Eqs. (35) and (36).

Proposition 4: Let $\mathbf{P}^*$, $\mathbf{W}^*$, and $\mathbf{S}^*$ be the optimal deployment, cell partitioning, and normalized flow matrix for the constrained optimization problem in Eqs. (35) and (36). Then,

$$p_n^* = \tilde{p}_n + \Gamma_n^* \times \min\left(1, \frac{\gamma_n}{\zeta_n \|\Gamma_n^*\|}\right), \ \forall n \in \mathcal{I}_{\mathcal{A}} \bigcup \mathcal{I}_{\mathcal{F}} \tag{37}$$

where $\Gamma_n^* = z_n^* - \tilde{p}_n$.

The proof of Proposition 4 is provided in Appendix F. Based on the optimal condition in Proposition 4, we design the Lifetime-Optimized Routing-aware Lloyd (LORL) Algorithm to optimize the deployment in heterogeneous multi-hop WSNs with network lifetime constraint. Given an initial deployment $\tilde{\mathbf{P}}$, LORL Algorithm iterates between three steps: (i) update the cell partitioning $\mathbf{W}$ according to Eq. (23); (ii) update the normalized flow matrix $\mathbf{S}$ using Bellman-Ford Algorithm; and (iii) update the deployment $\mathbf{P}$ according to Eq. (37). The algorithm continues until the stop criterion $\frac{\mathcal{D}_{\text{old}} - \mathcal{D}_{\text{new}}}{\mathcal{D}_{\text{old}}} \geq \epsilon$ is satisfied, where $\mathcal{D}_{\text{old}}$ and $\mathcal{D}_{\text{new}}$ are the cost functions in the previous and current iterations, respectively. The proof of convergence for the LORL algorithm is similar to that of other Lloyd-like algorithms [37].

VII. Experiments

Simulations are carried out for a heterogeneous wireless sensor network consisting of 30 APs and 3 FCs. We consider a square field of size 10km $\times$ 10km, i.e., $\Omega = [0, 10000]^2$. Simulations are performed for two different sensor density functions, a uniform distribution $f(\omega) = \frac{1}{\int_\Omega d\omega} = 10^{-8}$ and a mixture of Gaussian where sensors are distributed according to:

$$\begin{aligned} f(\omega) = \frac{1}{2} \times \mathcal{N}\left(\begin{bmatrix}\mu_1^{(1)}\\ \mu_2^{(1)}\end{bmatrix}, \begin{bmatrix}\Sigma_{1,1}^{(1)} & 0\\ 0 & \Sigma_{2,2}^{(1)}\end{bmatrix}\right) \\ + \frac{1}{4} \times \mathcal{N}\left(\begin{bmatrix}\mu_1^{(2)}\\ \mu_2^{(2)}\end{bmatrix}, \begin{bmatrix}\Sigma_{1,1}^{(2)} & 0\\ 0 & \Sigma_{2,2}^{(2)}\end{bmatrix}\right) \\ + \frac{1}{4} \times \mathcal{N}\left(\begin{bmatrix}\mu_1^{(3)}\\ \mu_2^{(3)}\end{bmatrix}, \begin{bmatrix}\Sigma_{1,1}^{(3)} & 0\\ 0 & \Sigma_{2,2}^{(3)}\end{bmatrix}\right), \end{aligned}$$

where $\mu_1^{(1)} = 3,000$, $\mu_2^{(1)} = 3,000$, $\Sigma_{1,1}^{(1)} = 1.5 \times 10^6$, $\Sigma_{2,2}^{(1)} = 1.5 \times 10^6$, $\mu_1^{(2)} = 6,000$, $\mu_2^{(2)} = 7,000$, $\Sigma_{1,1}^{(2)} = 2 \times 10^6$, $\Sigma_{2,2}^{(2)} = 2 \times 10^6$, $\mu_1^{(3)} = 7,500$, $\mu_2^{(3)} = 2,500$, $\Sigma_{1,1}^{(3)} = 10^6$, $\Sigma_{2,2}^{(3)} = 10^6$. All homogeneous densely deployed sensors share the transmitter antenna gain of $G_{t_{\text{sensor}}} = 1$. We consider a radio bit-rate of $R_b = 1$Mbps and assume that the wavelength of the carrier signal is $\lambda_c = 0.3$m. In order for APs and FCs to receive the signal without error, the received power at each point $n \in \mathcal{I}_{\mathcal{A}} \bigcup \mathcal{I}_{\mathcal{F}}$ should be greater than some threshold P_{th_n}. Moreover, the transceiver electronics in each AP n consumes ρ_n J/bit for digital coding, modulation, and filtering before signal transmission. Table II summarizes the values of P_{th_n} and ρ_n for all APs and FCs [16].

Let us denote the transmitter antenna gain of AP n by G_{t_n}. In addition, for each point $n \in \mathcal{I}_{\mathcal{A}} \bigcup \mathcal{I}_{\mathcal{F}}$, let G_{r_n} be its receiver antenna gain. Table III summarizes the values of the transmitter and receiver antenna gains for all nodes [16].

Note that parameters η_i and $\beta_{i,j}$, for all $i \in \mathcal{I}_{\mathcal{A}}$ and $j \in \mathcal{I}_{\mathcal{A}} \bigcup \mathcal{I}_{\mathcal{F}}$, can be calculated using the explained experimental setup. For example, we have $\eta_7 = \frac{P_{th_7} \times (4\pi)^2}{R_b G_{t_{\text{sensor}}} G_{r_7} \lambda_c^2} = \frac{10^{-8} \times (4\pi)^2}{10^6 \times 1 \times 2 \times (0.3)^2} = 8.77$ pJ/bit/m^2 and $\beta_{10,20} = \frac{P_{th_{20}} \times (4\pi)^2}{R_b G_{t_{10}} G_{r_{20}} \lambda_c^2} = \frac{6 \times 10^{-9} \times (4\pi)^2}{10^6 \times 2 \times 2 \times (0.3)^2} = 2.63$ pJ/bit/m^2. For performance evaluation, 10 initial AP and FC deployments are generated randomly on Ω, i.e., the location of each node is generated according to a uniform distribution on Ω. The maximum number of iterations for all algorithms is set to 200 and the Lagrangian multiplier is set to $\lambda = 0.25$.

TABLE IV: Weighted power comparison for the uniform sensor density function

CF	Global	GSA	HTTL	MWCDS	PSO	Rhombus	SHMS	RL
15.49	14.98	17.28	12.80	17.12	19.98	16.21	22.39	**10.12**

TABLE V: Weighted power comparison for the mixture of Gaussian sensor density function

CF	Global	GSA	HTTL	MWCDS	PSO	Rhombus	SHMS	RL
7.07	6.81	9.49	6.23	9.38	9.97	14.65	16.62	**5.58**

A. Static Heterogeneous Multi-Hop WSNs

We compare the total weighted communication power consumption of our proposed RL Algorithm with Cluster-Formation (CF) Algorithm [39], Global Algorithm [40], Gradient-SA (GSA) Algorithm [33], HTTL Algorithm [7], MWCDS Algorithm [41], PSO Algorithm [42], Rhombus Algorithm [24], and SHMS Algorithm [43]. To reduce the number of hops that data packets have to travel to reach the fusion centers, the Cluster-Formation algorithm employs a graph theoretic approach to optimize both the number of clusters and their corresponding diameters. The Global algorithm deploys network nodes such that the average Euclidean distance between access points and their corresponding fusion centers is minimized. Starting with a dense triangular grid deployment, the GSA algorithm first removes those nodes with least coverage; then, it moves the boundary nodes toward the gradient direction that maximizes the covered area. For a two-tier hierarchy of APs and FCs, the HTTL algorithm iteratively updates the deployment, cell partitioning, and connections between APs and FCs while the flow of data from each sensor to its corresponding FC is mediated by exactly one access point. MWCDS Algorithm aims to deploy the minimum number of network nodes such that the resulting network is both connected and energy efficient. PSO is a population-based iterative algorithm for finding the optimal deployment and minimizing the non-linear objective function. Rhmobus Algorithm uses a rhombus-based grid search for an energy-aware deployment that maximizes the coverage as well. For a given deployment, the SHMS algorithm determines the connections between APs and FCs such that the maximum energy consumed by each network node is minimized.

The weighted power consumption of Cluster-Formation, Global, GSA, HTTL, MWCDS, PSO, Rhombus, SHMS, and RL algorithms for the uniform sensor density function are summarized in Table IV. The RL algorithm outperforms other algorithms and achieves a lower weighted communication power consumption. Note that although the HTTL algorithm proposed in [7] deploys nodes based on the necessary conditions of optimality, the network architecture is restricted to a two-tier hierarchy while the RL algorithm simultaneously optimizes over the deployment and data routing. As a result, the deployment based on the RL algorithm results in a WSN that saves about 21% of the energy compared to that of the HTTL Algorithm.

Table V summarizes the weighted communication power consumption of Cluster-Formation, Global, GSA, HTTL, MWCDS, PSO, Rhombus, SHMS, and RL algorithms for the mixture of Gaussian sensor density function. The RL algorithm results in a power consumption of 5.58 Watts and outperforms other methods. Furthermore, the RL algorithm leads to a network architecture that exhaust its available communication energy in a time period that is longer by about 10% of that of HTTL Algorithm, the second best algorithm.

B. Mobile Heterogeneous Multi-Hop WSNs with a Total Movement Energy Constraint

The underlying assumption in all deployment strategies studied in Section VII-A is that the optimal locations are calculated offline and then APs and FCs are placed at the corresponding positions. However, in many applications, e.g., when the target region is a hostile environment, static deployment is not feasible. Instead, network nodes are initially deployed in the target region, e.g., by airdropping them using drones or manual placement in an accessible sub-region of the field and then each AP or FC moves to its optimal location based on the initial deployment and available movement energy. When the total available movement energy is limited, which is the focus of this section, the optimization problem is translated into a resource allocation problem where the optimal energy supply for each AP or FC is determined such that the resulting total communication power consumption after optimal deployment is minimized. In Section VII-C, we study the performance evaluation when the available movement energy is predetermined and the optimization problem is translated to that of enhancing the network lifetime.

The same experimental setup described at the beginning of Section VII and in Tables II and III is used for the simulations. Furthermore, Table VI provides the moving cost parameters ζ_n for all $n \in \mathcal{I}_{\mathcal{A}} \bigcup \mathcal{I}_{\mathcal{F}}$. We consider a total available movement energy of $\gamma = 40,000$ Joules for the constrained objective function in Eqs. (27) and (28).

TABLE VI: Moving cost parameters (J/m)

$\zeta_{1:8}$	$\zeta_{9:22}$	$\zeta_{23:30}$	ζ_{31}	ζ_{32}	ζ_{33}
2	4	6	4	5	6

We compare the total weighted communication power consumption of our proposed MERL Algorithm with BCBS Algorithm [44], Lloyd-α Algorithm [12], OMF Algorithm [14], VCOND Algorithm [28], and VFA Algorithm [13]. BCBS Algorithm augments the iterative procedure of Lloyd Algorithm to maximize the network's coverage and minimize network nodes' movement. The Lloyd-α algorithm applies a penalty term to the Lloyd algorithm to reduce the movement steps and save traveling energy while guaranteeing the convergence property. The OMF algorithm optimizes the movement

TABLE VII: Weighted power comparison

Sensor Density Function	BCBS	Lloyd-α	OMF	VCOND	VFA	MERL
uniform	24.35	29.12	27.35	27.92	27.85	**14.49**
mixture of Gaussian	15.94	17.38	17.29	15.32	18.76	**7.64**

TABLE VIII: Movement energy constraints (J)

$\gamma_{1:8}$	$\gamma_{9:22}$	$\gamma_{23:30}$	γ_{31}	γ_{32}	γ_{33}
800	1100	1400	2000	2400	2600

plan for nodes such that each region in the network has a minimum number of nodes to relay the data to fusion centers while the sum of network nodes' traveling distances is minimized. The VCOND algorithm iteratively partitions the target region according to the Voronoi diagram and relocates each network node based on the net virtual force coming from vertices and edges of its corresponding Voronoi cell. The VFA algorithm uses attractive and repulsive virtual forces on nodes such that not only every two network nodes in the final deployment maintain a minimum distance from each other, but also the communication distances are minimized by avoiding network nodes to be located very far from each other. For a fair comparison, the same initial deployment is used for all algorithms.

The weighted communication power consumption of BCBS, Lloyd-α, OMF, VCOND, VFA, and MERL algorithms for the uniform sensor density function are summarized in Table VII. All algorithms exhausted the available movement energy γ to move the AP and FC nodes from their initial deployment to their designated optimal locations. The MERL algorithm leads to a deployment that consumes communication energy in a rate that is almost half of other algorithms. The superior performance of the MERL algorithm is due to the optimal energy allocation among APs and FCs, as it is implicit in Eq. (31). Note that if the total movement energy γ is large enough, e.g., $\gamma \geq \sum_{i=1}^{N+M} \zeta_i \|\tilde{p}_i - z_i^*\|$, then the performance of the MERL algorithm will converge to that of the RL algorithm. However, since the value of γ in our experiments is not large enough, some APs and FCs will run out of their allocated movement energy and MERL algorithm leads to a communication power consumption that is larger than that of the RL algorithm in Section VII-A.

Table VII also summarizes the weighted communication power consumption of BCBS, Lloyd-α, OMF, VCOND, VFA, and MERL algorithms for the mixture of Gaussian sensor density function. The MERL algorithm significantly outperforms other methods and leads to a communication power consumption that is less than half of what other algorithms achieve. This is because the MERL algorithm can optimally adapt to any underlying sensor density function $f(\omega)$ and deploy APs and FCs accordingly, as we studied in Section V.

C. Mobile Heterogeneous Multi-Hop WSNs with a Network Lifetime Constraint

While we studied the performance evaluation of mobile WSNs under a total movement energy constraint in Section VII-B, here, we focus on enhancing the network lifetime, which necessitates APs and FCs to have individual movement energy constraints, as formulated in Eqs. (35) and (36). We use the same experimental setup as described at the beginning of Section VII and in Tables II, III, and VI for performance evaluation. In addition, Table VIII provides the maximum individual movement energy consumption γ_n for all $n \in \mathcal{I}_{\mathcal{A}} \bigcup \mathcal{I}_{\mathcal{F}}$.

We compare the weighted communication power consumption of our proposed LORL Algorithm with those of BCBS Algorithm, Lloyd-α Algorithm, OMF Algorithm, and VFA Algorithm described in Section VII-B. For a fair comparison, the same initial deployment as in Section VII-B is used for all algorithms.

The weighted communication power consumption of BCBS, Lloyd-α, OMF, VCOND, VFA, and LORL algorithms for the uniform sensor density function are provided in Table IX. The LORL algorithm outperforms other methods and achieves a significantly lower power consumption. For instance, the LORL algorithm leads to a deployment in which the network consumes its residual energy with a rate that is less than 70% of that of the VFA algorithm. This in turn prolongs the network lifetime, which is a prominent factor in wireless sensor networks.

Table IX also summarizes the power consumption of different algorithms for the mixture of Gaussian sensor density function. LORL Algorithm achieves a power consumption of 9.59 Watts and outperforms other methods. Fig. 2 shows the final deployment of different algorithms where APs and FCs are denoted by red squares and black circles, respectively.

The sum of individual movement energies in Table VIII, i.e. $\sum_{i=1}^{N+M} \gamma_i$, is equal to the value of γ in Section VII-B. In other words, Table VIII represents one exemplary distribution of the total movement energy γ among APs and FCs; however, it is different from the optimal energy allocation provided by the MERL algorithm in Section VII-B. The results in Tables VII and IX verify that the MERL algorithm achieves a lower total power consumption compared to the LORL algorithm although it does not guaranttee any individual power constraint.

VIII. Conclusion

In this work, a heterogeneous multi-hop wireless sensor network is discussed where data is collected from densely deployed sensors and transferred to heterogeneous fusion centers using heterogeneous access points as relay nodes. We modeled the minimum communication power consumption of such networks as an optimization problem and studied the necessary conditions of optimal deployment under both static and mobile network settings. A novel generalized Voronoi diagram is proposed to provide the best cell partition for the heterogeneous multi-hop network. When manual deployment is feasible, the necessary conditions of optimal deployment are explored under the static network setup and accordingly

TABLE IX: Weighted power comparison

Sensor Density Function	BCBS	Lloyd-α	OMF	VCOND	VFA	LORL
uniform	28.74	27.64	30.12	29.78	25.24	**17.33**
mixture of Gaussian	20.21	17.24	20.12	16.55	14.60	**9.59**

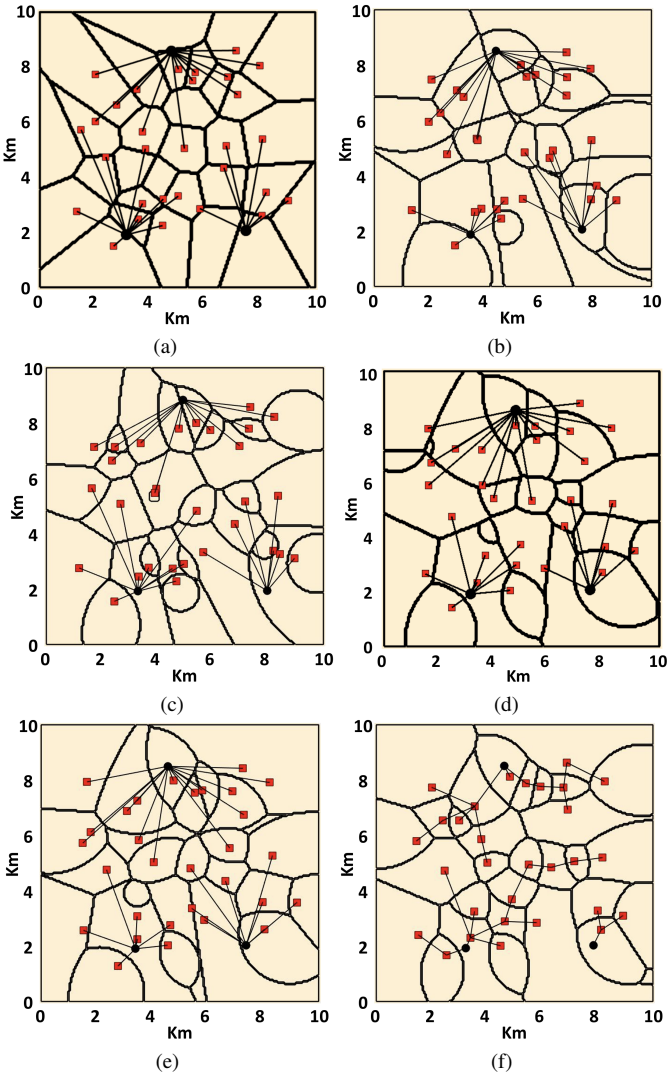

Fig. 2: Node deployment for different algorithms and the mixture of Gaussian sensor density function. (a) BCBS (b) Lloyd-α (c) OMF (d) VCOND (e) VFA (f) LORL.

a Routing-aware Lloyd algorithm is proposed for deployment. However, when static placement is not possible, the necessary conditions of the optimal deployment are studied under a mobile network setting where APs and FCs move from their initial locations to their optimal positions. We consider both total and individual movement energy constraints and formulate them as resource allocation and lifetime optimizations, respectively. Based on the derived necessary conditions, we propose Movement-Efficient Routing-aware Lloyd and Lifetime-Optimized Routing-aware Lloyd algorithms to deploy APs and FCs under total and individual energy constraints, respectively. Simulation results show that our proposed RL, MERL, and LORL algorithms significantly save communication power in such networks and provide superior results compared to other methods in the literature.

Appendix A

Proof of Lemma 1: The AP power coefficient $g_n(\mathbf{P},\mathbf{S})$ defined in Eq. (12) is the power consumption for transmitting 1 bit data from AP n to the FCs. This includes both the transmission power at each AP, including AP n, on the paths connecting AP n to the FCs, and the receiver power at each AP, excluding AP n, on the paths connecting AP n to the FCs. Since $R_b \int_{W_n} f(\omega)d\omega$ is the total amount of data collected by AP n from sensors within the region W_n in a unit time, the term $g_n(\mathbf{P},\mathbf{S})\, R_b \int_{W_n} f(\omega)d\omega$ is the required communication power for transmitting the sensory data collected within the region W_n from AP n to the FCs. Hence, the left-hand-side of Eq. (14) is the required communication power for transmitting the sensory data collected within the target region from APs to FCs. This can be decomposed into the APs' total transmission power in addition to the required receiver power for the data to reach FCs from APs. This proves Eq. (14) since the right-hand-side of Eq. (14) can be rewritten as $\overline{\mathcal{P}}_{\mathcal{A}}^{T} + \sum_{i=1}^{N}\sum_{j=1}^{N} \rho_j F_{i,j}(\mathbf{W},\mathbf{S})$, i.e., the sum of APs' total transmission power and the receiver power for all links (i,j) connecting AP i and AP j. ■

Appendix B

Proof of Proposition 1: Using Eq. (15), we have:

$$\begin{aligned}
\mathcal{D}(\mathbf{P},\mathbf{W},\mathbf{S}) &= \sum_{n=1}^{N}\int_{W_n}\Big(\eta_n\|p_n-\omega\|^2 R_b + \lambda g_n(\mathbf{P},\mathbf{S})\, R_b \\
&\qquad + \lambda\rho_n R_b\Big) f(\omega)d\omega \\
&\geq \sum_{n=1}^{N}\int_{W_n}\min_j\Big(\eta_j\|p_j-\omega\|^2 R_b + \lambda g_j(\mathbf{P},\mathbf{S})\, R_b \\
&\qquad + \lambda\rho_j R_b\Big) f(\omega)d\omega \\
&= \int_{\Omega}\min_j\Big(\eta_j\|p_j-\omega\|^2 R_b + \lambda g_j(\mathbf{P},\mathbf{S})\, R_b \\
&\qquad + \lambda\rho_j R_b\Big) f(\omega)d\omega \\
&= \sum_{n=1}^{N}\int_{\mathcal{V}_n}\min_j\Big(\eta_j\|p_j-\omega\|^2 R_b + \lambda g_j(\mathbf{P},\mathbf{S})\, R_b \\
&\qquad + \lambda\rho_j R_b\Big) f(\omega)d\omega \\
&= \sum_{n=1}^{N}\int_{\mathcal{V}_n}\Big(\eta_n\|p_n-\omega\|^2 R_b + \lambda g_n(\mathbf{P},\mathbf{S})\, R_b \\
&\qquad + \lambda\rho_n R_b\Big) f(\omega)d\omega \\
&= \mathcal{D}(\mathbf{P},\mathcal{V}(\mathbf{P},\mathbf{S}),\mathbf{S}). \qquad (38)
\end{aligned}$$

Hence, the generalized Voronoi diagram provides the optimal cell partitioning for any given deployment $\mathbf{P}$ and normalized flow matrix $\mathbf{S}$. ■

APPENDIX C

Proof of Proposition 2: Eq. (23) is a direct implication of Proposition 1. Eq. (24) is directly followed from Eq. (19). Here, we prove Eq. (22) for the optimal locations of APs and FCs. First, we study the shape of the Voronoi regions in (16). Note that the Voronoi regions defined in Eq. (16) have the same formulation as the generalized Voronoi diagram defined in Eq. (7) in [7], i.e., both of them can be expressed as $\mathcal{V}_n = \{\omega | a_n \|p_n - \omega\|^2 + b_n \leq a_k \|p_k - \omega\|^2 + b_k, \forall k \neq n\}$, where the coefficients a_i and b_i are constants independent of the value of ω. Therefore, the same reasoning as in Appendix D in [7] shows that Proposition 1 in [10] holds for the Voronoi cells defined in Eq. (16) as well. Now, using the parallel axis theorem [45], the heterogeneous multi-hop communication power consumption can be written as:

$$\begin{aligned}\mathcal{D}\left(\mathbf{P},\mathbf{W},\mathbf{S}\right) &= \sum_{n=1}^{N}\int_{W_n}\eta_n\|c_n-\omega\|^2 R_b f(\omega)d\omega \\ &+ \sum_{n=1}^{N}\eta_n\|p_n-c_n\|^2 R_b v_n \\ &+ \lambda\sum_{i=1}^{N}\sum_{j=1}^{N+M}\beta_{i,j}\|p_i-p_j\|^2 F_{i,j}\left(\mathbf{W},\mathbf{S}\right) \\ &+ \lambda\sum_{n=1}^{N}\rho_n\left[\sum_{i=1}^{N}F_{i,n}\left(\mathbf{W},\mathbf{S}\right)+R_b\int_{W_n}f(\omega)d\omega\right], \end{aligned} \quad (39)$$

where $v_n = v\left(W_n\right)$ and c_n are the volume and centroid of the region W_n, respectively. Using Proposition 1 in [10], since the optimal deployment $\mathbf{P}^*$ should have a zero gradient, we take the partial derivatives of (39) with respect to AP and FC locations. For each $i \in \mathcal{I}_A$, we have

$$\begin{aligned}\frac{\partial\mathcal{D}}{\partial p_i^*} &= 2\eta_i(p_i^*-c_i^*)R_b v_i^* + 2\lambda\sum_{j=1}^{N+M}\beta_{i,j}(p_i^*-p_j^*)F_{i,j}^* \\ &+ 2\lambda\sum_{j=1}^{N}\beta_{j,i}(p_i^*-p_j^*)F_{j,i}^* = 0, \end{aligned} \quad (40)$$

and for each $i \in \mathcal{I}_{\mathcal{F}}$, we have

$$\frac{\partial\mathcal{D}}{\partial p_i^*} = 2\lambda\sum_{j=1}^{N}\beta_{j,i}(p_i^*-p_j^*)F_{j,i}^* = 0. \quad (41)$$

By solving Eqs. (40) and (41), we obtain Eq. (22) and the proof is complete. ■

APPENDIX D

Proof of Lemma 2: Before going through the proof, we state the following lemma:

Lemma 3: Given a set of points $q_i \in \mathbb{R}^2$ and non-negative scalar weights a_i for $i \in \{1,\cdots,K\}$, and a scalar m, the geometric locus of the point $p \in \mathbb{R}^2$ such that the equality

$$\sum_{i=1}^{K} a_i\|p-q_i\|^2 = m \quad (42)$$

holds, is either an empty set, a single point, or a circle centered at the point $c = \frac{\sum_{i=1}^{K} a_i q_i}{\sum_{i=1}^{K} a_i}$.

Proof: Let $p = (p_x, p_y)$ and $q_i = (q_{i,x}, q_{i,y})$. Then, we can rewrite Eq. (42) as

$$\begin{aligned}&\left(\sum_{i=1}^{K}a_i\right)\left(p_x^2+p_y^2\right) - 2\left(\sum_{i=1}^{K}a_i q_{i,x}\right)p_x - 2\left(\sum_{i=1}^{K}a_i q_{i,y}\right)p_y \\ &= m - \sum_{i=1}^{K} a_i\|q_i\|^2. \end{aligned} \quad (43)$$

By manipulating both sides, we can rewrite Eq. (43) as follows:

$$\begin{aligned}&\left[p_x - \frac{\sum_{i=1}^{K}a_i q_{i,x}}{\sum_{i=1}^{K}a_i}\right]^2 + \left[p_y - \frac{\sum_{i=1}^{K}a_i q_{i,y}}{\sum_{i=1}^{K}a_i}\right]^2 \\ &= \frac{m - \sum_{i=1}^{K} a_i\|q_i\|^2}{\sum_{i=1}^{K}a_i} + \frac{\left(\sum_{i=1}^{K}a_i q_{i,x}\right)^2 + \left(\sum_{i=1}^{K}a_i q_{i,y}\right)^2}{\left(\sum_{i=1}^{K}a_i\right)^2}. \end{aligned} \quad (44)$$

Hence, the geometric locus of the point $p = (p_x, p_y)$ is an empty set or a single point if the right-hand-side of Eq. (44) is negative or zero, respectively; otherwise, the geometric locus is a circle centered at the point $c = \frac{\sum_{i=1}^{K} a_i q_i}{\sum_{i=1}^{K} a_i}$ with the radius $r = \sqrt{\frac{m-\sum_{i=1}^{K} a_i\|q_i\|^2}{\sum_{i=1}^{K}a_i} + \frac{\left(\sum_{i=1}^{K}a_i q_{i,x}\right)^2+\left(\sum_{i=1}^{K}a_i q_{i,y}\right)^2}{\left(\sum_{i=1}^{K}a_i\right)^2}}$, and Lemma 3 is proved.

Corollary 1: If the geometric locus in Lemma 3 is a circle centered at c with radius r, then for any point p within this circle we have $\sum_{i=1}^{K} a_i\|p-q_i\|^2 < m$, i.e., moving the point p inside this circle reduces the weighted squared sum in Eq. (42).

Now, assume that there exists at least one AP or FC, say n, for which Eq. (29) in Lemma 2 does not hold for an optimal deployment $\mathbf{P}^*$, cell partitioning $\mathbf{W}^*$, and normalized flow matrix $\mathbf{S}^*$, i.e., p_n^* does not lie on the segment $\overline{z_n^*\tilde{p}_n}$. We aim to find another deployment such as $\mathbf{P}'$, $\mathbf{W}'$, and $\mathbf{S}'$ so that $E\left(\mathbf{P}'\right) \leq \gamma$ and $\mathcal{D}\left(\mathbf{P}',\mathbf{W}',\mathbf{S}'\right) < \mathcal{D}\left(\mathbf{P}^*,\mathbf{W}^*,\mathbf{S}^*\right)$; hence, contradicting the optimality assumption of $\mathbf{P}^*$, $\mathbf{W}^*$, and $\mathbf{S}^*$, and concluding that Eq. (29) holds for all APs and FCs. For this purpose, let $\mathbf{W}' = \mathbf{W}^*$, $\mathbf{S}' = \mathbf{S}^*$, and $p_i' = p_i^*$ for all $i \in \mathcal{I}_{\mathcal{A}} \bigcup \mathcal{I}_{\mathcal{F}} \backslash \{n\}$. We aim to determine the location p_n' accordingly. Using the parallel axis theorem [45], we have:

$$\mathcal{D}\left(\mathbf{P}^*,\mathbf{W}^*,\mathbf{S}^*\right) = \sum_{i=1}^{N}\int_{W_i^*}\eta_i\|c_i^*-\omega\|^2 R_b f(\omega)d\omega$$

$$+\sum_{i=1}^{N}\eta_i R_b v_i^*\|p_i^*-c_i^*\|^2$$
$$+\lambda\sum_{i=1}^{N}\sum_{j=1}^{N+M}\beta_{i,j}\|p_i^*-p_j^*\|^2F_{i,j}\left(\mathbf{W}^*,\mathbf{S}^*\right)$$
$$+\lambda\overline{\mathcal{P}}_{\mathcal{A}}^{R}\left(\mathbf{W}^*,\mathbf{S}^*\right), \tag{45}$$

where v_i^* and c_i^* are the volume and centroid of the region W_i^*, respectively. In what follows, we assume that $n\in\mathcal{I}_{\mathcal{A}}$, i.e. point n is an AP. Similar proof can be carried out for $n\in\mathcal{I}_{\mathcal{F}}$. Note that Eq. (45) can be split as $\mathcal{D}\left(\mathbf{P}^*,\mathbf{W}^*,\mathbf{S}^*\right)=\mathcal{D}_1\left(\mathbf{P}^*,\mathbf{W}^*,\mathbf{S}^*\right)+\mathcal{D}_2\left(\mathbf{P}^*,\mathbf{W}^*,\mathbf{S}^*\right)$, where

$$\mathcal{D}_1(\mathbf{P}^*,\mathbf{W}^*,\mathbf{S}^*)=\eta_n R_b v_n^*\|p_n^*-c_n^*\|^2$$
$$+\sum_{j=1}^{N+M}\lambda\beta_{n,j}F_{n,j}^*\|p_n^*-p_j^*\|^2$$
$$+\sum_{j=1}^{N}\lambda\beta_{j,n}F_{j,n}^*\|p_n^*-p_j^*\|^2, \tag{46}$$

i.e., $\mathcal{D}_1$ includes those terms in Eq. (45) that involve p_n^*. In particular, regardless of the point n's position, we have $\mathcal{D}_2\left(\mathbf{P}^*,\mathbf{W}^*,\mathbf{S}^*\right)=\mathcal{D}_2\left(\mathbf{P}',\mathbf{W}',\mathbf{S}'\right)$. According to Lemma 3, the geometric locus of points such as p_n^* for which the value of $\mathcal{D}_1\left(\mathbf{P}^*,\mathbf{W}^*,\mathbf{S}^*\right)$ in Eq. (46) remains the same is a circle Φ_n^* centered at the point $z_n^*=z_n\left(\mathbf{P}^*,\mathbf{W}^*,\mathbf{S}^*\right)$ defined in Eq. (20), with radius $r_n^*=\|z_n^*-p_n^*\|$. Note that if $\|z_n^*-\tilde{p}_n\|<\|z_n^*-p_n^*\|$, then setting $p_n'=\tilde{p}_n$ not only leads to the movement energy $E\left(\mathbf{P}'\right)<E\left(\mathbf{P}^*\right)$, but also results in $\mathcal{D}_1\left(\mathbf{P}',\mathbf{W}',\mathbf{S}'\right)<\mathcal{D}_1\left(\mathbf{P}^*,\mathbf{W}^*,\mathbf{S}^*\right)$ since p_n' lies inside Φ_n^*. Therefore, we have $\mathcal{D}\left(\mathbf{P}',\mathbf{W}',\mathbf{S}'\right)<\mathcal{D}\left(\mathbf{P}^*,\mathbf{W}^*,\mathbf{S}^*\right)$ which is in contradiction with the optimality of $\mathbf{P}^*$, $\mathbf{W}^*$, and $\mathbf{S}^*$; hence, we have $\|z_n^*-\tilde{p}_n\|\geq\|z_n^*-p_n^*\|$. Let $\hat{p}_n$ be the intersection point of the circle Φ_n^* and segment $\overline{z_n^*\tilde{p}_n}$. Since $\|\tilde{p}_n-\hat{p}_n\|<\|\tilde{p}_n-p_n^*\|$, there exists an $\epsilon_n\in\mathbb{R}^+$ such that $\|\tilde{p}_n-\hat{p}_n\|+\epsilon_n<\|\tilde{p}_n-p_n^*\|$. If $p_n'=\hat{p}_n+\epsilon_n\times\frac{z_n^*-\hat{p}_n}{\|z_n^*-\hat{p}_n\|}$, then not only do we have $E\left(\mathbf{P}'\right)<E\left(\mathbf{P}^*\right)$ since $E\left(\mathbf{P}^*\right)-E\left(\mathbf{P}'\right)>\zeta_n\epsilon_n>0$, but also $\mathcal{D}_1\left(\mathbf{P}',\mathbf{W}',\mathbf{S}'\right)<\mathcal{D}_1\left(\mathbf{P}^*,\mathbf{W}^*,\mathbf{S}^*\right)$ since p_n' lies inside the circle Φ_n^*. Therefore, we have $\mathcal{D}\left(\mathbf{P}',\mathbf{W}',\mathbf{S}'\right)<\mathcal{D}\left(\mathbf{P}^*,\mathbf{W}^*,\mathbf{S}^*\right)$ which contradicts the optimality of $\mathbf{P}^*$, $\mathbf{W}^*$, and $\mathbf{S}^*$ and concludes the proof. ■

APPENDIX E

Proof of Proposition 3: If $p_i^*=z_i^*$ for all $i\in\mathcal{I}_d$, then Eq. (28) implies that $E\left(\mathbf{P}^*\right)=\sum_{i\in\mathcal{I}_d}\zeta_i\|\Gamma_i^*\|\leq\gamma$; hence, Eq. (31) reduces to the trivial statement $p_n^*=\tilde{p}_n+\Gamma_n^*$ and the proof is complete. Therefore, we assume that there exists at least one point, say n, for which $p_n^*\neq z_n^*$. Note that if any residual movement energy is left in the optimal deployment, i.e., $E\left(\mathbf{P}^*\right)<\gamma$, then there exists an $\epsilon\in\mathbb{R}^+$ such that $E\left(\mathbf{P}^*\right)+\epsilon<\gamma$ and $\overline{p}_n=p_n^*+\epsilon\times\frac{z_n^*-p_n^*}{\|z_n^*-p_n^*\|}$ lies inside the circle centered at z_n^* and radius $\|z_n^*-p_n^*\|$. Then, according to Lemma 3 and Corollary 1, by fixing the cell partitioning, normalized flow matrix and the location of all points except point n, and placing point n at $\overline{p}_n$ we can achieve a lower total multi-hop communication power without exhausting the available movement energy, which contradicts the optimality of $\mathbf{P}^*$, $\mathbf{W}^*$, and $\mathbf{S}^*$. Therefore, $p_n^*\neq z_n^*$ implies that $E\left(\mathbf{P}^*\right)=\gamma$. Now, given the optimal deployment $\mathbf{P}^*$, $\mathbf{W}^*$, and $\mathbf{S}^*$, we construct the deployment $\mathbf{P}'$, $\mathbf{W}'$, and $\mathbf{S}'$ as follows. Let $\mathbf{W}'=\mathbf{W}^*$, $\mathbf{S}'=\mathbf{S}^*$, and $p_i'=p_i^*$ for all $i\in\mathcal{I}_{\mathcal{A}}\bigcup\mathcal{I}_{\mathcal{F}}\backslash\{m,n\}$. Let $\epsilon_m,\epsilon_n\in\mathbb{R}^+$ be small values and define

$$p_m'=p_m^*-\epsilon_m\times\frac{z_m^*-\tilde{p}_m}{\|z_m^*-\tilde{p}_m\|}\ ,\ p_n'=p_n^*+\epsilon_n\times\frac{z_n^*-\tilde{p}_n}{\|z_n^*-\tilde{p}_n\|}. \tag{47}$$

To satisfy the equality $E\left(\mathbf{P}'\right)=\gamma$, we have $\zeta_n\epsilon_n=\zeta_m\epsilon_m$. Now, we calculate the change in the multi-hop communication power, i.e. $\mathcal{D}\left(\mathbf{P}',\mathbf{W}',\mathbf{S}'\right)-\mathcal{D}\left(\mathbf{P}^*,\mathbf{W}^*,\mathbf{S}^*\right)$. Assume that point m is fixed at p_m^* and we move point n from p_n^* to p_n'. Note that this movement only changes the term $\mathcal{D}_1$ defined in Eq. (46); thus, according to Lemma 3 and Eq. (44), this change is proportional to the difference between the squared radii, i.e.,

$$\Delta_1=\left[\|p_n'-z_n^*\|^2-\|p_n^*-z_n^*\|^2\right]\times\psi_n^*, \tag{48}$$

where ψ_n^* is defined in Eq. (32). Now, with point n placed at p_n', we move point m from p_m^* to p_m'. Similar to the above argument, the term Δ_2 defined as

$$\Delta_2=\left[\|p_m'-z_m^*\|^2-\|p_m^*-z_m^*\|^2\right]\times\psi_m^* \tag{49}$$

captures the change in $\mathcal{D}$ with the assumption that point n was located at p_n^*. Now, we take into account that point n was located at p_n' instead of p_n^* during point m's movement.

$$\Delta_3=\lambda\beta_{n,m}F_{n,m}^*\times\Big[\left(\|p_n'-p_m'\|^2-\|p_n'-p_m^*\|^2\right)$$
$$-\left(\|p_n^*-p_m'\|^2-\|p_n^*-p_m^*\|^2\right)\Big] \tag{50}$$
$$=\lambda\beta_{n,m}F_{n,m}^*\times\Big[\left(\|p_n'-p_m^*\|^2+\epsilon_m^2\right.$$
$$\left.-2\epsilon_m\|p_n'-p_m^*\|\cos\measuredangle p_n'p_m^*p_m'-\|p_n'-p_m^*\|^2\right)$$
$$-\left(\|p_n^*-p_m'\|^2-\|p_n^*-p_m'\|^2-\epsilon_m^2\right.$$
$$\left.-2\epsilon_m\|p_n^*-p_m'\|\cos\measuredangle p_n^*p_m'\tilde{p}_m\right)\Big] \tag{51}$$
$$=\lambda\beta_{n,m}F_{n,m}^*\times\left[2\epsilon_m^2-2\epsilon_m\left(\epsilon_m-\epsilon_n\cos\theta\right)\right] \tag{52}$$
$$=\lambda\beta_{n,m}F_{n,m}^*\times\left[2\frac{\zeta_m}{\zeta_n}\epsilon_m^2\cos\theta\right], \tag{53}$$

where s and $\theta=\measuredangle z_n^*sz_m^*$ are the intersection point and the angle between the lines $\overline{z_n^*\tilde{p}_n}$ and $\overline{z_m^*\tilde{p}_m}$, respectively. Note that in Eq. (50), without any loss of generality, we have assumed that the direction of the flow of data, if any, is from point n to point m. Moreover, Eq. (51) follows from the law of cosines and Eq. (53) follows from the equation $\zeta_n\epsilon_n=\zeta_m\epsilon_m$. Hence, we have:

$$\mathcal{D}\left(\mathbf{P}',\mathbf{W}',\mathbf{S}'\right)-\mathcal{D}\left(\mathbf{P}^*,\mathbf{W}^*,\mathbf{S}^*\right)=\Delta_1+\Delta_2+\Delta_3$$
$$=\left[\frac{\zeta_m^2}{\zeta_n^2}\epsilon_m^2-2\frac{\zeta_m}{\zeta_n}\epsilon_m\|p_n^*-z_n^*\|\right]\times\psi_n^* \tag{54}$$
$$+\left[\epsilon_m^2+2\epsilon_m\|p_m^*-z_m^*\|\right]\times\psi_m^*+2\lambda\beta_{n,m}F_{n,m}^*\frac{\zeta_m}{\zeta_n}\epsilon_m^2\cos\theta.$$

Due to the optimality of $\mathbf{P}^*$, $\mathbf{W}^*$, and $\mathbf{S}^*$, Eq. (54) should be non-negative, or equivalently:

$$\epsilon_m \left(\frac{\zeta_m^2}{\zeta_n^2}\psi_n^* + \psi_m^* + 2\lambda\beta_{n,m}F_{n,m}^* \frac{\zeta_m}{\zeta_n}\cos\theta \right) \geq 2\left(\frac{\zeta_m}{\zeta_n}\psi_n^* \|p_n^* - z_n^*\| - \psi_m^* \|p_m^* - z_m^*\| \right). \quad (55)$$

According to Eq. (32), the term $\lambda\beta_{n,m}F_{n,m}^*$ is included in both ψ_n^* and ψ_m^*, i.e. $\psi_n^* \geq \lambda\beta_{n,m}F_{n,m}^*$ and $\psi_m^* \geq \lambda\beta_{n,m}F_{n,m}^*$; therefore, we have:

$$\begin{aligned} &\frac{\zeta_m^2}{\zeta_n^2}\psi_n^* + \psi_m^* + 2\lambda\beta_{n,m}F_{n,m}^* \frac{\zeta_m}{\zeta_n}\cos\theta \\ &\geq \frac{\zeta_m^2}{\zeta_n^2}\lambda\beta_{n,m}F_{n,m}^* + \lambda\beta_{n,m}F_{n,m}^* + 2\lambda\beta_{n,m}F_{n,m}^* \frac{\zeta_m}{\zeta_n}\cos\theta \\ &\geq \lambda\beta_{n,m}F_{n,m}^* \left(\frac{\zeta_m}{\zeta_n} - 1 \right)^2 \geq 0, \end{aligned} \quad (56)$$

thus, the term inside the parentheses on the left hand side of Eq. (55) is always non-negative. Note that if the right hand side of Eq. (55) is strictly positive, then we can choose a small enough ϵ_m such that the inequality in Eq. (55) is contradicted. Hence, we have:

$$\zeta_m\psi_n^*\|p_n^* - z_n^*\| \leq \zeta_n\psi_m^*\|p_m^* - z_m^*\|. \quad (57)$$

By swapping the indices m and n in Eq. (47) and repeating the same argument, we have:

$$\zeta_m\psi_n^*\|p_n^* - z_n^*\| \geq \zeta_n\psi_m^*\|p_m^* - z_m^*\|. \quad (58)$$

Eqs. (57) and (58) imply that:

$$\zeta_m\psi_n^*\|p_n^* - z_n^*\| = \zeta_n\psi_m^*\|p_m^* - z_m^*\|. \quad (59)$$

Note that Eq. (47) indicates that Eq. (57) holds for any n but only for a dynamic index $m \in \mathcal{I}_d$, and similarly Eq. (58) holds for any m but only for a dynamic index $n \in \mathcal{I}_d$. Hence, Eqs. (57) and (59) imply that $\chi_m^* \geq \chi_n^*$ if $n \in \mathcal{I}_s, m \in \mathcal{I}_d$ and $\chi_m^* = \chi_n^*$ if $n, m \in \mathcal{I}_d$, and Eq. (30) is proved. Now, by using Eq. (59) and the equality $E(\mathbf{P}^*) = \gamma$, we can write:

$$\begin{aligned} &\sum_{i\in\mathcal{I}_d} \zeta_i\|\Gamma_i^*\| - \gamma = \sum_{i\in\mathcal{I}_d} \zeta_i\|p_i^* - z_i^*\| = \sum_{i\in\mathcal{I}_d} \frac{\zeta_i^2\psi_n^*}{\zeta_n\psi_i^*}\|p_n^* - z_n^*\| \\ &= \frac{\psi_n^*}{\zeta_n}\|p_n^* - z_n^*\| \sum_{i\in\mathcal{I}_d} \frac{\zeta_i^2}{\psi_i^*}, \end{aligned} \quad (60)$$

or equivalently:

$$\|p_n^* - z_n^*\| = \frac{\sum_{i\in\mathcal{I}_d} \zeta_i\|\Gamma_i^*\| - \gamma}{\frac{\psi_n^*}{\zeta_n}\sum_{i\in\mathcal{I}_d} \frac{\zeta_i^2}{\psi_i^*}}. \quad (61)$$

Hence, we have:

$$\begin{aligned} p_n^* &= \tilde{p}_n + \frac{\Gamma_n^*}{\|\Gamma_n^*\|}\left(\|\Gamma_n^*\| - \|p_n^* - z_n^*\|\right) \\ &= \tilde{p}_n + \Gamma_n^* \left(1 - \frac{\sum_{i\in\mathcal{I}_d} \zeta_i\|\Gamma_i^*\| - \gamma}{\|\Gamma_n^*\| \times \frac{\psi_n^*}{\zeta_n} \times \sum_{i\in\mathcal{I}_d} \frac{\zeta_i^2}{\psi_i^*}} \right), \end{aligned} \quad (62)$$

and the proof is complete. ■

APPENDIX F

Proof of Proposition 4: If $p_n^* = z_n^*$ in an optimal deployment $\mathbf{P}^*$, $\mathbf{W}^*$, and $\mathbf{S}^*$, then Eq. (36) implies that $E_n(\mathbf{P}^*) = \zeta_n\|\Gamma_n^*\| \leq \gamma_n$. Therefore, Eq. (37) reduces to the trivial statement $p_n^* = \tilde{p}_n + \Gamma_n^*$ and the proof is complete. Hence, we assume that $p_n^* \neq z_n^*$. Now, if any residual movement energy is left in point n, i.e. if $E_n(\mathbf{P}^*) < \gamma_n$, then there exists an $\epsilon_n \in \mathbb{R}^+$ such that $E_n(\mathbf{P}^*) + \epsilon_n < \gamma_n$ and the point $\overline{p}_n = p_n^* + \epsilon_n \times \frac{z_n^* - p_n^*}{\|z_n^* - p_n^*\|}$ lies inside the circle centered at z_n^* with radius $\|z_n^* - p_n^*\|$. Then, according to Lemma 3, by fixing the cell partitioning, normalized flow matrix and the location of all APs and FCs except point n, and placing point n at $\overline{p}_n$, we can achieve a lower total multi-hop communication power without exhausting the available movement energy in point n, which contradicts the optimality of $\mathbf{P}^*$, $\mathbf{W}^*$, and $\mathbf{S}^*$. Therefore, $p_n^* \neq z_n^*$ implies that $E_n(\mathbf{P}^*) = \gamma_n$, that is

$$\zeta_n\|p_n^* - \tilde{p}_n\| = \gamma_n. \quad (63)$$

According to Lemma 2, we have

$$p_n^* = \delta_n\tilde{p}_n + (1 - \delta_n) z_n^*, \quad (64)$$

where $\delta_n \in [0, 1]$, which indicates that

$$\|p_n^* - \tilde{p}_n\| = (1 - \delta_n)\|z_n^* - \tilde{p}_n\|. \quad (65)$$

Eqs. (63) and (65) imply that $\delta_n = 1 - \frac{\gamma_n}{\zeta_n\|z_n^* - \tilde{p}_n\|}$. Therefore, Eq. (64) can be written as:

$$\begin{aligned} p_n^* &= \left(1 - \frac{\gamma_n}{\zeta_n\|z_n^* - \tilde{p}_n\|} \right)\tilde{p}_n + \left(\frac{\gamma_n}{\zeta_n\|z_n^* - \tilde{p}_n\|} \right) z_n^* \\ &= \tilde{p_n} + \left(\frac{\gamma_n}{\zeta_n\|z_n^* - \tilde{p}_n\|} \right)(z_n^* - \tilde{p}_n) \\ &= \tilde{p}_n + \frac{\gamma_n}{\zeta_n\|\Gamma_n^*\|}\Gamma_n^*. \end{aligned} \quad (66)$$

Eqs. (63) and (64) imply that $\gamma_n = \zeta_n\|p_n^* - \tilde{p}_n\| \leq \zeta_n\|z_n^* - \tilde{p}_n\| = \zeta_n\|\Gamma_n^*\|$, i.e., $\frac{\gamma_n}{\zeta_n\|\Gamma_n^*\|} \leq 1$. Thus, Eq. (66) can be rewritten as $p_n^* = \tilde{p}_n + \min\left(1, \frac{\gamma_n}{\zeta_n\|\Gamma_n^*\|}\right)\Gamma_n^*$ which concludes the proof. ■

REFERENCES

[1] J. Guo, S. Karimi-Bidhendi, and H. Jafarkhani, "Energy-efficient node deployment in wireless ad-hoc sensor networks," in *ICC 2020-2020 IEEE International Conference on Communications (ICC)*, pp. 1–6, IEEE, Jun 2020.

[2] J. Guo, E. Koyuncu, and H. Jafarkhani, "A source coding perspective on node deployment in two-tier networks," *IEEE Transactions on Communications*, vol. 66, pp. 3035–3049, Feb 2018.

[3] J. Cortes, S. Martinez, and F. Bullo, "Spatially-distributed coverage optimization and control with limited-range interactions," *ESAIM: Control, Optimisation and Calculus of Variations*, vol. 11, pp. 691–719, Oct 2005.

[4] M. Benaddy, B. El Habil, M. El Ouali, O. El Meslouhi, and S. Krit, "A mutlipath routing algorithm for wireless sensor networks under distance and energy consumption constraints for reliable data transmission," in *2017 International Conference on Engineering & MIS (ICEMIS)*, pp. 1–4, IEEE, May 2017.

[5] S. Karimi-Bidhendi, J. Guo, and H. Jafarkhani, "Using quantization to deploy heterogeneous nodes in two-tier wireless sensor networks," in *2019 IEEE International Symposium on Information Theory (ISIT)*, pp. 1502–1506, IEEE, Jul 2019.

[6] Y. T. Hou, Y. Shi, H. D. Sherali, and S. F. Midkiff, "On energy provisioning and relay node placement for wireless sensor networks," *IEEE Transactions on Wireless Communications*, vol. 4, pp. 2579–2590, Nov 2005.

[7] S. Karimi-Bidhendi, J. Guo, and H. Jafarkhani, "Energy-efficient node deployment in heterogeneous two-tier wireless sensor networks with limited communication range," *IEEE Transactions on Wireless Communications*, vol. 20, no. 1, pp. 40–55, 2020.

[8] M. Noori and M. Ardakani, "Design of heterogeneous sensor networks with lifetime and coverage considerations," *IEEE Wireless Communications Letters*, vol. 1, pp. 193–196, Mar 2012.

[9] J. Guo, P. Walk, and H. Jafarkhani, "Optimal deployments of uavs with directional antennas for a power-efficient coverage," *IEEE Transactions on Communications*, vol. 68, pp. 5159–5174, Aug 2020.

[10] J. Guo and H. Jafarkhani, "Sensor deployment with limited communication range in homogeneous and heterogeneous wireless sensor networks," *IEEE Transactions on Wireless Communications*, vol. 15, pp. 6771–6784, Jul 2016.

[11] J. Guo and H. Jafarkhani, "Movement-efficient sensor deployment in wireless sensor networks with limited communication range," *IEEE Transactions on Wireless Communications*, vol. 18, pp. 3469–3484, May 2019.

[12] Y. Song, B. Wang, Z. Shi, K. R. Pattipati, and S. Gupta, "Distributed algorithms for energy-efficient even self-deployment in mobile sensor networks," *IEEE Transactions on Mobile Computing*, vol. 13, pp. 1035–1047, Apr 2013.

[13] Y. Zou and K. Chakrabarty, "Sensor deployment and target localization in distributed sensor networks," *ACM Transactions on Embedded Computing Systems (TECS)*, vol. 3, pp. 61–91, Feb 2004.

[14] S. Chellappan, W. Gu, X. Bai, D. Xuan, B. Ma, and K. Zhang, "Deploying wireless sensor networks under limited mobility constraints," *IEEE Transactions on Mobile Computing*, vol. 6, pp. 1142–1157, Aug 2007.

[15] H. Yousefi'zadeh, H. Jafarkhani, and M. Moshfeghi, "Power optimization of wireless media systems with space-time block codes," *IEEE Transactions on Image Processing*, vol. 13, pp. 873–884, Jun 2004.

[16] W. B. Heinzelman, *Application-specific protocol architectures for wireless networks*. PhD thesis, Massachusetts Institute of Technology, Jun 2000.

[17] M. A. Razzaque and S. Dobson, "Energy-efficient sensing in wireless sensor networks using compressed sensing," *Sensors*, vol. 14, pp. 2822–2859, Feb 2014.

[18] J. Wu and S. Yang, "Optimal movement-assisted sensor deployment and its extensions in wireless sensor networks," *Simulation Modelling Practice and Theory*, vol. 15, pp. 383–399, Apr 2007.

[19] Z. Xinlian and Q. Wenhao, "Sensor network energy saving sleep scheduling algorithm research," in *2014 International Conference on Information and Communications Technologies (ICT 2014)*, pp. 1–5, May 2014.

[20] V. Kawadia and P. Kumar, "Power control and clustering in ad hoc networks," in *IEEE INFOCOM 2003. Twenty-second Annual Joint Conference of the IEEE Computer and Communications Societies (IEEE Cat. No. 03CH37428)*, vol. 1, pp. 459–469, IEEE, Mar 2003.

[21] Y. Yoo and D. Agrawal, "Mobile sensor relocation to prolong the lifetime of wireless sensor networks," in *VTC spring 2008-IEEE vehicular technology conference*, pp. 193–197, IEEE, 2008.

[22] M. R. Senouci, A. Mellouk, and A. Aissani, "Random deployment of wireless sensor networks: a survey and approach," *International Journal of Ad Hoc and Ubiquitous Computing*, vol. 15, no. 1-3, pp. 133–146, 2014.

[23] M. R. Senouci, A. Mellouk, and A. Aissani, "An analysis of intrinsic properties of stochastic node placement in sensor networks," in *2012 IEEE Global Communications Conference (GLOBECOM)*, pp. 494–499, IEEE, 2012.

[24] R. Singh and M. S. Manu, "An energy efficient grid based static node deployment strategy for wireless sensor networks," *International Journal of Electronics and Information Engineering*, vol. 7, no. 1, pp. 32–40, 2017.

[25] M. Maksimović and V. Milošević, "Evaluating the optimal sensor placement for smoke detection," *Yugoslav journal of operations research*, vol. 26, no. 1, pp. 33–50, 2016.

[26] X. Deng, Z. Yu, R. Tang, X. Qian, K. Yuan, and S. Liu, "An optimized node deployment solution based on a virtual spring force algorithm for wireless sensor network applications," *Sensors*, vol. 19, no. 8, p. 1817, 2019.

[27] C. Liu, Z. Zhao, W. Qu, T. Qiu, and A. K. Sangaiah, "A distributed node deployment algorithm for underwater wireless sensor networks based on virtual forces," *Journal of Systems Architecture*, vol. 97, pp. 9–19, 2019.

[28] M. S. Ghahroudi, A. Shahrabi, and T. Boutaleb, "Voronoi-based cooperative node deployment algorithm in mobile sensor networks," in *2020 IEEE 91st Vehicular Technology Conference (VTC2020-Spring)*, pp. 1–5, IEEE, 2020.

[29] Y. Su, L. Guo, Z. Jin, and X. Fu, "A voronoi-based optimized depth adjustment deployment scheme for underwater acoustic sensor networks," *IEEE Sensors Journal*, vol. 20, no. 22, pp. 13849–13860, 2020.

[30] H. Mahboubi and A. G. Aghdam, "Distributed deployment algorithms for coverage improvement in a network of wireless mobile sensors: Relocation by virtual force," *IEEE Transactions on Control of Network Systems*, vol. 4, no. 4, pp. 736–748, 2016.

[31] B. Cao, J. Zhao, Z. Lv, X. Liu, X. Kang, and S. Yang, "Deployment optimization for 3d industrial wireless sensor networks based on particle swarm optimizers with distributed parallelism," *Journal of Network and Computer Applications*, vol. 103, pp. 225–238, 2018.

[32] S. K. Gupta, P. Kuila, and P. K. Jana, "Genetic algorithm for k-connected relay node placement in wireless sensor networks," in *Proceedings of the second international conference on computer and communication technologies*, pp. 721–729, Springer, 2016.

[33] Y. El Khamlichi, A. Tahiri, A. Abtoy, I. Medina-Bulo, and F. Palomo-Lozano, "A hybrid algorithm for optimal wireless sensor network deployment with the minimum number of sensor nodes," *Algorithms*, vol. 10, no. 3, p. 80, 2017.

[34] J.-H. Chang and L. Tassiulas, "Energy conserving routing in wireless ad-hoc networks," in *Proceedings IEEE INFOCOM 2000. Conference on Computer Communications. Nineteenth Annual Joint Conference of the IEEE Computer and Communications Societies (Cat. No. 00CH37064)*, vol. 1, pp. 22–31, IEEE, Mar 2000.

[35] R. Bellman, "On a routing problem," *Quarterly of applied mathematics*, vol. 16, pp. 87–90, Apr 1958.

[36] S. Lloyd, "Least squares quantization in pcm," *IEEE transactions on information theory*, vol. 28, pp. 129–137, Mar 1982.

[37] S. Karimi-Bidhendi, J. Guo, and H. Jafarkhani, "Energy-efficient node deployment in static and mobile heterogeneous multi-hop wireless sensor networks," *arXiv preprint arXiv:2101.04780*, 2021.

[38] G. Wang, M. J. Irwin, P. Berman, H. Fu, and T. La Porta, "Optimizing sensor movement planning for energy efficiency," in *Proceedings of the 2005 international symposium on Low power electronics and design*, pp. 215–220, Aug 2005.

[39] P. Chatterjee and N. Das, "Multiple sink deployment in multi-hop wireless sensor networks to enhance lifetime," in *2015 Applications and Innovations in Mobile Computing (AIMoC)*, pp. 48–54, IEEE, Feb 2015.

[40] Z. Vincze, R. Vida, and A. Vidacs, "Deploying multiple sinks in multi-hop wireless sensor networks," in *IEEE international conference on pervasive services*, pp. 55–63, IEEE, Jul 2007.

[41] D. Djenouri and M. Bagaa, "Energy-aware constrained relay node deployment for sustainable wireless sensor networks," *IEEE Transactions on Sustainable Computing*, vol. 2, no. 1, pp. 30–42, 2017.

[42] D. R. Dandekar and P. Deshmukh, "Energy balancing multiple sink optimal deployment in multi-hop wireless sensor networks," in *2013 3rd IEEE International Advance Computing Conference (IACC)*, pp. 408–412, IEEE, Feb 2013.

[43] T. K. Jain, D. S. Saini, and S. V. Bhooshan, "Lifetime optimization of a multiple sink wireless sensor network through energy balancing," *Journal of Sensors*, vol. 2015, Jan 2015.

[44] W. Fang, X. Song, X. Wu, J. Sun, and M. Hu, "Novel efficient deployment schemes for sensor coverage in mobile wireless sensor networks," *Information Fusion*, vol. 41, pp. 25–36, 2018.

[45] B. Paul, *Kinematics and dynamics of planar machinery*. Prentice Hall, Jun 1979.